



1 The Hestia Fossil Fuel CO₂ Emissions Data Product for the Los 2 Angeles Megacity (Hestia-LA)

3 Kevin R. Gurney¹, Risa Patarasuk⁴, Jianming Liang^{2,3}, Yang Song², Darragh O’Keeffe⁵, Preeti
4 Rao⁶, James R. Whetstone⁷, Riley M. Duren⁸, Annmarie Eldering⁸, Charles Miller⁸

5 ¹School of Informatics, Computing, and Cyber Systems, Northern Arizona University, Flagstaff, AZ, USA

6 ²School of Life Sciences, Arizona State University, Tempe AZ USA

7 ³Now at ESRI, Redlands, CA USA

8 ⁴Citrus County, Dept. of Systems Management, Lecanto, FL, USA

9 ⁵Contra Costa County, Department of Information Technology, Martinez, CA, USA

10 ⁶School for Environment and Sustainability, University of Michigan, Ann Arbor, MI, USA

11 ⁷National Institute for Standards and Technology, Gaithersburg, MD, USA

12 ⁸NASA Jet Propulsion Laboratory, California Institute of Technology, Pasadena, CA, USA

13 *Correspondence to:* Kevin R. Gurney (kevin.gurney@nau.edu)

14 **Abstract.** As a critical constraint to atmospheric CO₂ inversion studies, bottom-up spatiotemporally-explicit
15 emissions data products are necessary to construct comprehensive CO₂ emission information systems useful for
16 trend detection and emissions verification. High-resolution bottom-up estimation is also useful as a guide to
17 mitigation options, offering details that can increase mitigation efficiency and synergize with other policy goals at
18 the national to sub-urban spatial scale. The ‘Hestia Project’ is an effort to provide bottom-up fossil fuel (FFCO₂)
19 emissions at the urban scale with building/street and hourly space-time resolution. Here, we report on the latest
20 urban area for which a Hestia estimate has been completed – the Los Angeles Megacity, encompassing five
21 counties: Los Angeles County, Orange County, Riverside County, San Bernardino County and Ventura County. We
22 provide a complete description of the methods used to build the Hestia FFCO₂ emissions data product which is
23 presented on a 1 km x 1 km grid for the years 2010-2015. We find that the LA Basin emits 48.06 (± 5.3) MtC/yr,
24 dominated by the onroad sector. Because of the uneven spatial distribution of emissions, 10% of the largest emitting
25 gridcells account for 93.6%, 73.4%, 66.2%, and 45.3% of the industrial, commercial, onroad, and residential sector
26 emissions, respectively. Hestia FFCO₂ emissions are 10.7% larger than the inventory estimate generated by the local
27 metropolitan planning agency, a difference that is driven by the industrial and electricity production sectors. The
28 Hestia-LA v2.5 emissions data product can be downloaded from the data repository at the National Institute of
29 Standards and Technology (<https://doi.org/10.18434/T4/1502503>).

30 1 Introduction

31 Driven by the growth of fossil fuel combustion, the amount of carbon dioxide (CO₂), the most important
32 anthropogenic greenhouse gas (GHG) in the Earth’s atmosphere, recently reached an annual average global mean
33 concentration of 402.8 ± 0.1 parts per million (ppm) on its way to doubling pre-industrial levels (IPCC, 2013;
34 LeQuere et al., 2018). We have also witnessed the first time that the majority of world’s inhabitants reside in urban
35 areas. This trend, like atmospheric CO₂ levels, is intensifying. Projections show cities worldwide could add 2 to 3
36 billion people this century and are projected to triple in area by 2030 (UN DESA 1015; Seto et al., 2012).



37 These two thresholds are linked—almost three-quarters of energy-related, atmospheric CO₂ emissions are driven by
38 urban activity (Seto et al., 2014). If the world’s top 50 emitting cities were counted as one country, that nation would
39 rank third in emissions behind China and the United States (World Bank 2010). Indeed, urbanization is a factor
40 shaping national contributions to internationally agreed emission reductions, as subnational governments are playing
41 an increasing role in climate mitigation and adaptation policy implementation (Bulkeley 2010; Hsu et al., 2017).
42 Furthermore, the pace of urbanization continues to increase and opportunities to avoid carbon “lock-in” - where
43 relationships between technology, infrastructure, and urban form dictate decades of high-CO₂ development - are
44 diminishing (Ürge-Vorsatz et al., 2018; Seto et al., 2016; Erickson et al., 2015).

45 Motivated by these numerical realities and the recognition that low-emission development is consistent with a
46 variety of other co-benefits (e.g. air quality improvement), cities are taking steps to mitigate their CO₂ emissions
47 (Rosenzweig et al., 2010; Hsu et al., 2015; Watts 2017). For example, 9120 cities representing over 770 million
48 people (10.5% of global population) have committed to the Global Covenant of Mayors (GCoM) to promote and
49 support action to combat climate change (GCoM, 2018). Over 90 large cities, as part of the C40 network, have
50 similarly committed to mitigation actions with demonstrable progress. However, the scale of actual reductions
51 remains modest, despite the many pledges and initial progress. For example, a recent study reviewed 228 cities
52 pledged to reduce 454 megatons of CO₂ per year by 2020 (Erickson and Lazarus, 2012). Were they to meet these
53 commitments, the reduction would account for about 3% of current global urban emissions and less than 1% of total
54 global emissions projected for 2020. More important, there is a need for timely information to manage and assess
55 the performance of implemented mitigation efforts and policies (Bellassen et al., 2015).

56 One of the barriers to targeting a deeper list of emission reduction activities is the limited amount of actionable
57 emissions information at scales where human activity occurs: individual buildings, vehicles, parks, factories and
58 power plants (Gurney et al., 2015). These are the scales at which interventions in CO₂-emitting activity must occur.
59 Hence, the emissions magnitude and driving forces of those emissions must be understood and quantified at the
60 “human” scale to make efficient (i.e. prioritizing the largest available emitting activities/locales) mitigation choices
61 and to capture the urban co-benefits that also occur at this scale (e.g. improve traffic congestion, walkability, green
62 space). Similarly, a key obstacle to assessing progress is a lack of independent atmospheric evaluation (ideally
63 consistent in space and time with the human-scale emissions mapping) (Duren and Miller 2011).

64 Existing methods and tools to account for urban emissions have been developed primarily in the non-profit
65 community (WRI/WBCSD, 2004; Fong et al., 2014). In spite of these important efforts, most cities lack
66 independent, comprehensive and comparable sources of data and information to drive and/or adjust these
67 frameworks. Furthermore, the existing tools and methods are designed at an aggregate level (i.e. whole city, whole
68 province), missing the most important scale—sub-city—and hence provide limited actionable information.

69 The scientific community has begun to build information systems aimed at providing independent assessment of
70 urban CO₂ emissions. Through a combination of atmospheric measurements, atmospheric transport modeling and
71 data-driven “bottom-up” estimation, the scientific community is exploring different methodologies, applications,
72 and uncertainty estimation of these approaches (Hutyra et al., 2014). Atmospheric monitoring includes ground-based
73 CO₂ concentration measurements (McKain et al., 2012; Djuricin et al., 2010; Miles et al., 2017; Turnbull et al.,



74 2015, Verhulst et al., 2017), ground-based eddy flux measurements (Christen 2014; Crawford and Christen 2014;
75 Grimmond et al., 2002; Menzer et al., 2015; Velasco and Roth 2010; Velasco et al., 2005), aircraft-based flux
76 measurements (Mays et al., 2009; Cambaliza et al., 2014; 2015) and whole-column abundances from both ground,
77 and space-based, remote sensing platforms (Wunch et al., 2009; Kort et al., 2012; Wong et al., 2015; Schwandner et
78 al., 2018).

79 “Bottom-up” approaches, by contrast, include a mixture of direct flux measurement, indirect measurement and
80 modeling. Common among the bottom-up approaches are those that include flux estimation based on a combination
81 of activity data (population, number of vehicles, building floor area) and emission factors (amount of CO₂ emitted
82 per activity), socioeconomic regression modeling, or scaling from aggregate fuel consumption (VandeWeghe and
83 Kennedy, 2007; Shu and Lam, 2011; Zhou and Gurney, 2011; Gurney et al., 2012; Jones and Kammen, 2014;
84 Ramaswami and Chavez, 2013; Patarasuk et al., 2016; Porse et al., 2016). Direct end-of-pipe flux monitoring is
85 often used for large point sources such as power plants (Gurney et al., 2016). Indirect fluxes (those occurring outside
86 of the domain of interest but driven by activity within) can be estimated through either direct atmospheric
87 measurement (and apportioned to the domain of interest) or can be modeled through process-based (Clark and
88 Chester 2017) or economic input-output models (Ramaswami et al., 2008).

89 Integration of bottom-up urban flux estimation with atmospheric monitoring has been achieved with atmospheric
90 inverse modeling, an approach whereby surface fluxes are estimated from a best fit between bottom-up estimation
91 and fluxes inferred, via atmospheric transport modeling, from atmospheric concentrations (Lauvaux et al., 2013;
92 Lauvaux et al., 2016; Breon et al., 2015; Davis et al., 2017). Though the various measurement and modeling
93 components continue to be tested, integration offers an urban anthropogenic CO₂ information system which can
94 provide accuracy, emissions process information, and spatiotemporal detail. This combination of attributes satisfies
95 a number of urgent requirements. For example, it can offer the means to evaluate urban emissions mitigation efforts
96 by assessing urban trends. Space, time, and process detail of emitting activity can guide mitigation efforts,
97 illuminating where efficient opportunities exist to maximize reductions or focus new efforts. Finally, emissions
98 quantification is also seen as a potentially powerful metric with which to better understand the urbanization process
99 itself, given the importance of energy consumption to the evolution of cities.

100 The Hestia Project was begun to estimate bottom-up urban fossil fuel CO₂ (FFCO₂) fluxes for use within integrated
101 flux information systems. Begun in the city of Indianapolis, the Hestia effort is now part of a larger experiment that
102 includes many of the modeling and measurement aspects described above. Referred to as the Indianapolis Flux
103 Experiment (INFLUX), this integrated effort has emerged to test and explore quantification and uncertainties of the
104 urban CO₂ and CH₄ measurement and modeling approaches using Indianapolis as the testbed experimental
105 environment (Whetstone et al., 2018; Davis et al., 2017).

106 Because urban areas differ in key attributes such as size, geography, and emission sector composition, multiple cities
107 are now being used to test aspects of anthropogenic CO₂ monitoring and modeling. The Hestia approach has been
108 used in a number of these urban domains. Here, we provide the methods and results from one of those urban domains,
109 the Los Angeles Basin Megacity. The Hestia-LA effort was developed under the Megacities Carbon framework
110 (<https://megacities.jpl.nasa.gov/portal/>). It was designed to serve the Megacities Carbon Project in a similar capacity



111 to its role in INFLUX. The Hestia-LA result is unique in that it is the first high-resolution spatiotemporally-explicit
112 inventory of FFCO₂ emissions centered over a megacity. A preliminary version of Hestia-LA containing only the
113 transportation sector emissions was reported by Rao et al. (2017). While emphasis thus far has been focused on
114 atmospheric CH₄ monitoring analyses in the LA megacity (Carranza et al., 2017; Wong et al., 2016; Verhulst et al.,
115 2017; Hopkins et al., 2016), work is ongoing to use the extensive atmospheric CO₂ observing capacity in the Los
116 Angeles domain (e.g. Newman et al., 2016; Feng et al., 2016; Wong et al., 2015; Wunch et al., 2009) within an
117 atmospheric CO₂ inversion.

118 In this paper, we describe the study domain, the input data, uncertainty, and the methods used to generate the Hestia-
119 LA (v2.5) data product and provide descriptive statistics at various scales of aggregation. We compare the Hestia
120 results to the metro region planning authority estimate and place the results in the context of urban greenhouse gas
121 mitigation. We discuss known gaps and weaknesses in the approach and goals for future work.

122 **2 Methods**

123 **2.1 Study Domain**

124 The Los Angeles metropolitan area is the second-largest metropolitan area in the United States and one of the largest
125 metropolitan areas in the world. Under the definition of the Metropolitan Statistical Area (MSA) by the U.S. Office
126 of Management and Budget, Metropolitan Los Angeles consists of Los Angeles and Orange counties with a land
127 area of 12,562 km² and a population of 9,819,000. The Greater Los Angeles Area, as a Combined Statistical Area
128 (CSA) defined by the U.S. Census Bureau, encompasses the three additional counties of Ventura, Riverside, and San
129 Bernardino with a total land area of 87,945 km² and an estimated population of 18,550,288 in 2014. The Hestia-LA
130 FFCO₂ emissions data product covers the complete geographic extent of these five counties including the Eastern,
131 relatively non-urbanized portions of San Bernardino and Riverside counties. Airport emissions associated with
132 aircraft up to 3000 feet are included as are marine shipping emissions out to 12 nautical miles from the coastal
133 boundary.

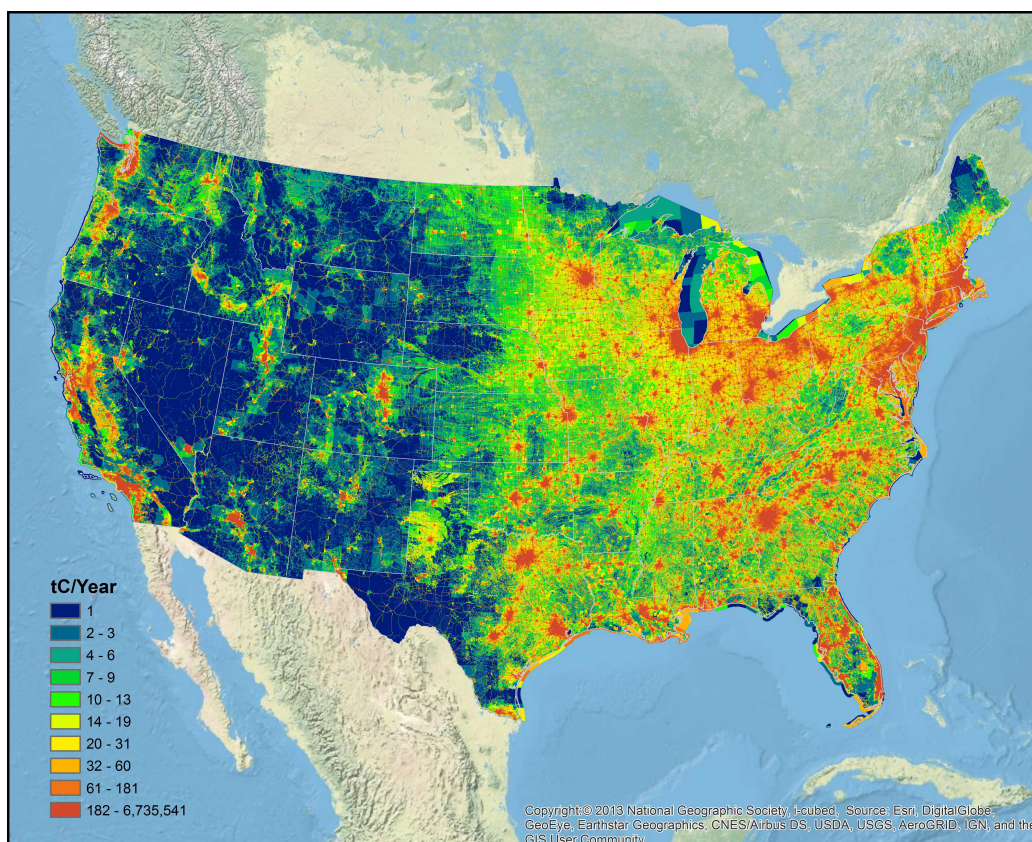


134

135 **Figure 1: The Hestia-LA urban domain**

136 **2.2 Input data**

137 Input data to the Hestia-LA data product are supplied by output of the Vulcan Project (Figure 2), a quantification of
138 FFCO₂ emissions at fine space and time scales for the entire US landscape (Gurney et al., 2009) The Hestia-LA
139 process extracts these results for the five counties within the Hestia-LA domain and adjusts these estimates where
140 superior local data are available and further downscales/distributes the Vulcan v3.0 results to buildings and street
141 segments. Details of the Vulcan v3.0 methodology is provided elsewhere (Gurney et al., 2018). Here, we summarize
142 the Vulcan v3.0 methods and then provide greater detail regarding the Hestia-LA processing of that data to high-
143 resolution space/time scales.



144

145 **Figure 2: Total annual FFCO₂ emissions for the year 2011 from the Vulcan v3.0 output.**

146 The Vulcan v3.0 input data (the output of which is the input for the Hestia-LA) are organized following nine
147 economic sector divisions (see Table 1) - residential, commercial, industrial, electricity production, onroad, nonroad,
148 railroad, commercial marine vessel, and airport. Also included are emissions associated with the calcining process in
149 the production of cement. The data sources within each sector are either acquired as FFCO₂ emissions (the onroad
150 sector and most of the nonroad and electricity production sectors) or as carbon monoxide (CO) emissions (all other
151 sectors) and transformed to FFCO₂ emissions via emission factors. Furthermore, the data sources are represented
152 geographically as either geocoded emitting locations (“point”) or as spatial aggregates (“nonpoint” or area-based
153 emissions). Point sources are stationary emitting entities identified to a geocoded location such as industrial facilities
154 in which emissions exit through a stack or identifiable exhaust feature (USEPA, 2015a). Area or nonpoint source
155 emissions are not inventoried at the facility-level but represent diffuse emissions within an individual U.S. county.
156 Because the focus of the current study is CO₂ emissions resulting from the combustion of a fossil fuels, fugitive or
157 evaporative emissions are not included nor are “process” emissions, for example, associated with high-temperature
158 metallurgical processes.

159 Much of the input data for Vulcan v3.0 are acquired from the Environmental Protection Agency’s (EPA) National
160 Emission Inventory (NEI) for the year 2011 (referred to hereafter as the “2011 NEI”) which is a comprehensive



161 inventory of all criteria air pollutants (CAPs) and hazardous air pollutants (HAPs) across the United States (USEPA,
162 2015b). All of the individual record-level reporting in the 2011 NEI comes with a source classification code (SCC)
163 which codifies the general emission technology, fuel type used, and sector (USEPA 1995).

164 FFCO₂ emissions from the electricity production sector are primarily retrieved from two sources other than the 2011
165 NEI. The first is the EPA's Clean Air Markets Division (CAMD) data (USEPA, 2015c) which reports FFCO₂
166 emissions at geocoded electricity production facility locations. The second is the Department of Energy's Energy
167 Information Administration (DOE EIA) reporting data (DOE/EIA, 2003) which reports fuel consumption at
168 geocoded electricity production facility locations. Some electricity production emissions are retrieved from the 2011
169 NEI (as CO emissions). Overlap between these three data sources is eliminated via preference in the order listed
170 above. A detailed comparison made between the CAMD and EIA FFCO₂ emissions along with greater detail
171 regarding data sources, data processing and procedures can be found in Quick et al., (2014) and Gurney et al. (2014;
172 2016; 2018).

173 The 2011 onroad FFCO₂ emissions are retrieved from the EMISSIONS FACTORS 2014 model (EMFAC2014), produced
174 by the California Air Resources Board (CARB 2014). Onroad transportation represents all mobile transport using
175 paved roadways and include both private and commercial vehicles of many individual classes (e.g., passenger
176 vehicles, buses, light duty trucks, etc). The nonroad sector, by contrast, includes all surface mobile vehicles that do
177 not travel on designated paved roads surface and include a large class of vehicles such as construction equipment
178 (e.g., bulldozers, backhoes, etc.), ATVs, snowmobiles, and airport fueling vehicles. The nonroad emissions are
179 derived from the 2011 NEI reporting of nonroad CO emissions. Airport emissions include all the emissions
180 emanating from aircraft during their taxi, takeoff, landing cycles up to 3000 feet and are derived from the 2011 NEI
181 point reporting. Other activities occurring at airports resulting in FFCO₂ emissions are captured in the commercial
182 building sector (building heating) or the nonroad sector (baggage vehicles), sourced to the 2011 NEI nonpoint, 2011
183 NEI point and 2011 NEI nonroad reporting. Railroad emissions include passenger and freight rail travel and are
184 sourced to the 2011 NEI nonpoint and point reporting. Commercial marine vessels (CMV) include all commercial-
185 based aquatic vessels on either ocean or freshwater sourced to the 2011 NEI nonpoint reporting. Personal aquatic
186 vehicles such as pleasure craft and sailboats are included in the nonroad sector. Emissions associated with cement
187 calcining are included given its potential size and the tradition of including it with CO₂ inventories and use
188 information from multiple sources (PCA, 2006; USGS, 2003; IPCC, 2006).

189 The FFCO₂ emissions input to the Hestia system from the Vulcan v3.0 output is associated with spatial elements
190 represented by points, lines and polygons, depending upon the data source, the sector and the available spatial proxy
191 data (Table 1). Further spatialization and temporalization occurs in the Hestia system.

192 **Table 1. Data sources used in the spatiotemporal distribution of FFCO₂ emissions (text provides acronym**
193 **explanations and sources).**

Sector/type	Emissions Data Source	Original spatial resolution/information	Spatial distribution	Temporal distribution
Onroad	EMFAC ^a , EPA NEI ^b onroad	County, road class, vehicle class	SCAG AADT ^c	PeMS ^d , CCS ^e
Electricity production	CAMD ^f CO ₂ , EIA ^g fuel, EPA NEI point CO	Lat/lon, fuel type, technology	EPA NEI Lat/Lon, Google Earth	CAMD, EIA and EPA



Residential nonpoint buildings	EPA NEI nonpoint CO	County, fuel type	SCAG Parcel, floor area, DOE RECS NE-EU ^h , LA County building footprint	eQUEST ⁱ
Nonroad	NEI nonpoint CO	County, vehicle class	EPA spatial surrogates (vehicle class specific)	EPA temporal surrogates (by SCC)
Airport	EPA NEI point CO	Lat/lon, aircraft class	Lat/Lon	LAWA ^k
Commercial nonpoint buildings	EPA NEI nonpoint CO	County, fuel	SCAG Parcel, floor area, DOE CBECs NE-EU ^l	eQUEST
Commercial point sources	EPA NEI point CO	Lat/lon, fuel type, combustion technology	EPA NEI Lat/Lon, Google Earth	eQUEST
Industrial point sources	EPA NEI point CO	Lat/Lon, fuel type, combustion technology	EPA NEI Lat/Lon, Google Earth	EPA temporal surrogates (by SCC)
Industrial nonpoint buildings	EPA NEI nonpoint CO	County, fuel type	SCAG-Parcel, floor area, DOE MECS NE-EU ^m	eQUEST
Commercial Marine Vessels	EPA NEI nonpoint CO	County, fuel type, port/underway	MEM ⁿ	MEM
Railroad	EPA NEI nonpoint CO, EPA NEI point CO	County, fuel type, segment	EPA NEI rail shapefile and density distribution	EPA temporal surrogates (by SCC)

194
195
196
197
198
199
200
201
202
203
204
205
206
207

- a. Emissions Factors Model
- b. Environmental Protection Agency, National Emissions Inventory
- c. Southern California Association of Governments, Annual Average Daily Traffic
- d. Performance Measurement System
- e. Continuous Count Stations
- f. Clean Air Markets Division
- g. Energy Information Administration
- h. Department of Energy Residential Energy Consumption Survey, non-electric energy use intensity
- i. Quick Energy Simulation Tool
- j. Source Classification Code
- k. Los Angeles World Airport
- l. Department of Energy Commercial Energy Consumption Survey, non-electric energy use intensity
- m. Department of Energy Manufacturing Energy Consumption Survey, non-electric energy use intensity
- n. Marine Emissions Model

208 To estimate FFCO₂ emissions as a multiyear time series from 2010 to 2015, the results for the year 2011 were scaled
 209 using sector/state/fuel consumption data (thermal units) from the DOE EIA (DOE/EIA, 2018). The electricity
 210 production sector was an exception to this approach where year-specific data was available in the CAMD and EIA
 211 data sources. Ratios were constructed relative to the year 2011 in all SEDS sector designations for each US state.
 212 The ratio values are applied to the annual totals in each of the sector/fuel categories specific to the state FIPS code.

213 2.3 Space/time processing

214 2.3.1 Residential, commercial, industrial nonpoint buildings

215 The general approach to spatializing the residential, commercial and industrial nonpoint FFCO₂ emissions is to
 216 allocate the county-scale, fuel-specific annual sector totals to individual buildings (or parcels) using data on building
 217 type, building age, total floor area, energy use intensity, and location.

218 A portion of the Hestia-LA building information were provided by the Southern California Association of
 219 Governments (SCAG) (SCAG, 2012) and included building type, age, floor area, and location. The spatial
 220 resolution of this information was at the land parcel scale (larger than the building footprint). Building footprint data
 221 was available in the county of Los Angeles only which offered additional building floor area information needed to
 222 correct some floor area values in the SCAG parcel data (LAC, 2016). For example, a large number of commercial
 223 parcels with zero floor area were found in the Riverside County data which were visually inspected in Google Earth
 224 to contain qualifying buildings. These floor area values were corrected through the combination of the Census
 225 block-group General Building Stock (GBS) database from the Federal Emergency Management Agency (FEMA)



226 (FEMA, 2017) and the National Land Cover Database 2011 (NLCD) which classifies the US land surface in 30m
227 pixels (Homer et al., 2015).

228 Building energy use intensity was derived from data gathered by the DOE EIA and the California Energy
229 Commission (CEC). The DOE EIA Commercial Buildings Energy Consumption Survey (CBECS), Manufacturing
230 Energy Consumption Survey (MECS), and Residential Energy Consumption Survey (RECS) represent regional
231 surveys of building energy consumption categorized by building type, fuel type, and age cohort (RECS, 2013;
232 CBECS, 2016; MECS, 2010). Data for the Pacific West Census Division was used and in the case of the commercial
233 sector, was appended by the CECs Commercial End-Use Survey (CEUS) data (CEC, 2006).

234 In the residential sector the non-electric energy use intensity (NE-EUI) was calculated from the reported energy
235 consumed and total floor area sampled specific to five building types (Table 2) in the 2009 RECS survey. This was
236 additionally categorized by fuel type (natural gas and fuel oil) and two age cohorts (pre-1980, post-1979).

237 **Table 2. Residential NE-EUI survey values by building type from the Residential Energy Consumption**
238 **Survey (RECS)**

RECS building type	Pre-1980 NG NE-EUI (kbtu/ft ²)	Post-1979 NG NE-EUI (kbtu/ft ²)	Pre-1980 Fuel oil NE-EUI (kbtu/ft ²)	Post-1979 Fuel oil NE-EUI (kbtu/ft ²)
Mobile home	52.56	22.90	NA*	NA
Single-family detached house	24.53	18.00	18.87	7.23
Single-family attached house	42.56	32.38	NA	NA
Apartment building with 2-4 units	27.84	42.27	NA	NA
Apartment building with 5 or more units	17.21	30.85	NA	NA

239 * "NA" – not applicable. This indicates that there was no fuel consumption of this type evident from the survey data.

240 In the commercial sector, the NE-EUI was similarly calculated from the 2012 CBECS energy consumption
241 microdata and total floor area sampled specific to twenty building types, two fuel types (natural gas and fuel oil) and
242 two age cohorts (pre-1980 and post-1979). However, the sampling for the two age cohorts was insufficient to
243 generate estimates and the age distinction was eliminated. Furthermore, where the sample sizes remained small, NE-
244 EUI data from the CEUS was used in place of CBECS estimates (7 of 20 building types qualified). As the CEUS
245 follows a building typology different from CBECS, a crosswalk of building types between the two datasets was
246 necessary (Table 3).

247 **Table 3. Building type crosswalk and NE-EUI values for commercial buildings derived from the CBECS and**
248 **CUES databases**

CBECS building class	CUES building class	NG NE-EUI (kbtu/ft ²)	Fuel oil NE-EUI (kbtu/ft ²)
Vacant	Miscellaneous	9.3	2.5
Office	All Offices	17.9*	1.67
Laboratory	Miscellaneous	174.7	0.93
Nonrefrigerated warehouse	Unrefrigerated Warehouse	3.1*	1.03
Food sales	Food Store	27.6*	2.5
Public order and safety	Miscellaneous	58.2	2.09
Outpatient health care	Health	29.1	3.05
Refrigerated warehouse	Refrigerated Warehouse	5.6*	2.5
Religious worship	Miscellaneous	35.7	0.00
Public assembly	Miscellaneous	26.5	0.23
Education	College, School	25.1*	1.7
Food service	Restaurant	210*	100.5
Inpatient health care	Health	113.9	2.6



Nursing	Health	67.4	1.2
Lodging	Lodging	42.4*	1.4
Strip shopping mall	Retail	62.7	2.5
Enclosed mall	Retail	4.8	0.02
Retail other than mall	Retail	13.6	16.7
Service	Miscellaneous	34.2	0.45
Other	Miscellaneous	18.5	5.3

249 * NE-EUI uses the CUES NE-EUI value due to sampling limitations in the CBECS data.

250 Unlike the commercial and residential survey data, the 2010 MECS survey data does not quantify energy
 251 consumption for individually sampled buildings but rather reports the sum of the sampled buildings within each
 252 census region categorized by manufacturing sector. The resulting NE-EUI values are shown in in Table 4. Like the
 253 commercial data, there was inadequate sampling to justify two age cohorts.

254 **Table 4. Industrial NE-EUI survey values from the DOE EIA MECS database**

MECS Class	NG NE-EUI (kbtu/ft ²)	Fuel oil NE-EUI (kbtu/ft ²)
Food	519.3	30.5
Beverage and Tobacco Products	162.4	8.5
Textile Mills	144.9	9.3
Textile Product Mills	63.4	0
Apparel	35.1	0
Leather and Allied Products	66.7	0
Wood Products	76.6	49.5
Paper	672.8	69.1
Printing and Related Support	96.6	0
Petroleum and Coal Products	9766.0	436.2
Chemicals	2126.3	17.9
Plastics and Rubber Products	124.7	2.4
Nonmetallic Mineral Products	556.0	48.9
Primary Metals	895.0	16.7
Fabricated Metal Products	124.2	2.3
Machinery	78.6	3.3
Computer and Electronic Products	80.0	0
Electrical Equip., Appliances, and Components	133.3	3.7
Transportation Equipment	100.6	4.0
Furniture and Related Products	28.6	0
Miscellaneous	44.7	2.8

255 The NE-EUI values derived from the CBECS/RECS/MECS and CEUS survey data reflect the total building fuel
 256 consumption for a specific fuel in a census region divided by the total floor area of all buildings in that census region
 257 consuming that fuel. This generates a mean building NE-EUI value. Actual buildings will vary around that mean
 258 value for a variety of reasons including different occupancy schedules, different energy efficiencies (in the envelope
 259 or heating/cooling system), different microclimate, and other physical/behavioral characteristics. Furthermore, the
 260 NE-EUI value applied in this way will not capture the reality that some buildings do not use fossil fuel (electricity-
 261 only buildings) or that some buildings use one fossil fuel only versus another or use a mix of fuels in a proportion
 262 different from the county total. Hence, each building will be allocated a mix of fossil fuel consumption identical to
 263 the county total.

264 **2.3.1.1 Spatial distribution**

265 The county-scale commercial, residential and industrial nonpoint FFCO₂ emissions are allocated to each land parcel
266 in proportion to the product of the NE-EUI and the total floor area,

$$267 \quad EC(b)_s^f = NE_EUI_s^f FA(b) \quad (1)$$

268 where the energy consumed, EC , in each building, b , is the product of the NE-EUI value, NE_EUI , and the floor
269 area, FA , for each fuel, f , and each building in sector, s . The total energy consumed, TEC , within the county for a
270 sector, s , is the sum of all the EC values across the N buildings in the sector,

$$271 \quad TEC_s^f = \sum_{b=1}^N EC(b)_s^f \quad (2)$$

272 To convert this to FFCO₂ emissions, we first calculate the fraction of the total energy consumption associated with
273 each building,

$$274 \quad F(b)_s^f = \frac{EC(b)_s^f}{TEC_s^f} \quad (3)$$

275 where, F is the fraction of TEC consumed in building, b , of sector s . This is then used to distribute the county total
276 FFCO₂ emissions as,

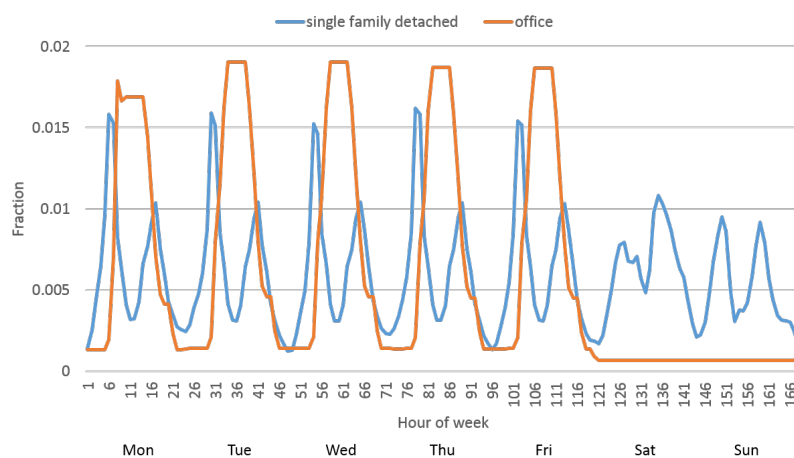
$$277 \quad E(b)_s^f = E_s^f F(b)_s^f \quad (4)$$

278 where E , is the FFCO₂ emissions either for the county or for building, b , and fuel. In allocating emissions from coal
279 consumptions, however, $NE-EUI$ takes the value of “1” for all building types so that the allocated emission in a
280 building is directly proportional to the floor area.

281 **2.3.1.2 Temporal distribution**

282 The hourly time structure for buildings in the residential and commercial sectors are created via the use of eQUEST,
283 a building energy simulation tool run for each of the building classes listed in Table 2 and Table 3 and using only
284 the temporal structure of the energy consumption output (*Hirsch & Associates, 2004*). The model domain is
285 specified as the city of Los Angeles for the year 2011 with TMY weather data from the DOE (*Marion and Urban,*
286 1995). The mean building area is provided by the parcel data as described previously.

287 For the industrial buildings, a temporal profile representing the mean of industrial point source temporal surrogates
288 provided by EPA, are used (USEPA, 2015a). Figure 3 shows the hourly time profile during a one-week period in
289 April for a selected building in the residential and commercial sector, respectively.



290

291 **Figure 3. Energy consumption intensity (hourly fraction) from an eQUEST simulation on the average week in**
 292 **2011 for two types of buildings: “single family detached house” and “office”.**

293 2.3.2 Industrial and commercial point sources

294 Little space/time processing is required for industrial and commercial point source emissions since they are
 295 geocoded to specific facilities/emitting stacks or similar identifiable emission points. However, visual inspection of
 296 the point source locations in GIS suggested potential geocoding errors. Point source locations were reviewed by
 297 searching facility names to an online address search or via the EPA’s Facility Registry Service (FRS) which can link
 298 the facility in question to all the reporting made to the federal government under other environmental regulations
 299 (USEPA, 2013). This often returns a more accurate physical location. The geolocations considered inaccurate were
 300 manually corrected. Out of the total 192 facilities with corrected locations, 13 were moved a distance of between
 301 924 and 1022 km while the remaining 179 were moved 0.5 km or less. The large magnitude location changes were
 302 likely transcription errors when originally recording the location coordinates.

303 A given commercial or industrial point source is typically composed of multiple emission processes or units. For
 304 example, in Los Angeles County, the 2011 NEI reports a total of 3409 emission records at 842 individual facilities.
 305 In some cases, the multiple emitting points at a facility are not at exactly the same geocoded point but may represent
 306 different emitting points at a facility that occupies a large area of land. Most often, however, all emitting points at a
 307 given facility are geocoded to the same latitude and longitude.

308 The sub-annual temporal distribution for the commercial and industrial point source emissions used temporal
 309 surrogate profiles provided by the EPA, linked according to the SCC of the emission record (USEPA, 2015a).

310 2.3.3 Electricity production

311 As described in Section 2.2, three different data sources are used to quantify the FFCO₂ emissions in the Hestia-LA
 312 domain: the Clean Air Markets Division (CAMD), the DOE-EIA reporting and 2011 NEI CO emissions data. In
 313 2011 there were a total of 34 CAMD facilities, 228 EIA facilities and 147 NEI facilities (reported through the NEI
 314 2011 point source fileset) in the Hestia-LA domain. Total electricity production emissions in the domain was 6.21



315 MtC/year exclusive of biogenic fuels and 6.68 MtC/year with biogenics included. The CAMD data is reported at
316 hourly resolution, while the DOE EIA data is reported at monthly resolution and the 2011 NEI data is reported at
317 annual resolution only. Reduction of all data to an hourly time increment was achieved by maintaining constant
318 emissions within a month or year for the DOE EIA and 2011 NEI data, respectively.

319 **2.3.4 Onroad**

320 A preliminary version of the Hestia-LA onroad emissions estimates were presented by Rao et al. (2017). The version
321 presented here uses updated data and Hestia methodologies.

322 **2.3.4.1 Temporal distribution**

323 The Hestia-LA onroad FFCO₂ emissions input are retrieved from the Vulcan v3.0 output spatialized to specific road
324 segments in the Hestia-LA domain and categorized by vehicle class/fuel. Hence, no further spatialization was
325 required.

326 Construction of the temporal distribution in the Hestia system relies upon the California Department of
327 Transportation (CalTrans) Performance Measurement System (PeMS) (PeMS, 2018). This dataset contains 2011
328 traffic count data collected at 5 min intervals at measuring stations along freeways and principal arterials and along
329 some minor arterials and collectors (major and minor). Aggregation of the 5-minute counts to hourly values are used
330 to construct hourly fractions for each measurement station.

331 To apply a time distribution for the FFCO₂ onroad emissions on each road segment, an Inverse Distance Weighting
332 (IDW) spatial interpolation method was used. A search within a neighborhood of a 10 km radius is performed from
333 the midpoint of each road segment to locate PeMS sites using a nearest neighbor searching library (Mount and Arya,
334 2010). In cases where more than one station was available, the IDW interpolation was applied; in cases where only
335 one station was available, the time structure of this station was directly assigned to the road segment in question. In
336 cases where no station was available within the 10-km neighborhood, an average temporal distribution was assigned
337 (an average of all station values in a county at that hour for that road type). This last case occurred mostly in the
338 rural portions of predominantly rural counties.

339 For local roads, PeMS data was not available in any of the counties within the Hestia-LA domain. Instead, the
340 weekday hourly time fractions were generated from Annual Average Weekday Traffic (AAWT) data supplied by
341 SCAG (*Mike Ainsworth*, 2014). The data contained five distinct time periods within a single 24 hour cycle: 6-9 am,
342 9 am-3 pm, 3-7 pm, 7-9 pm, 9 pm-6 am. Hourly time fractions for weekends were derived from the county average
343 of weekend hourly time fractions. The weekday and weekend hourly time fractions were combined to form a
344 complete week, and then replicated for all 52 weeks in the entire year. This was done because there was no
345 significant seasonality in weekday and weekend traffic across the year as observed from PeMS data.

346 **2.3.5 Nonroad**

347 The nonroad Hestia-LA FFCO₂ emissions are completely determined in the Vulcan system and hence, passed to the
348 Hestia-LA domain without further processing (see Gurney et al., 2018 for details). To summarize the Vulcan



349 process, California did not report FFCO₂ nonroad emissions to the NEI 2011 but did report nonroad CO emissions.
350 The CO emissions were converted to FFCO₂ using the SCC-specific ratios of CO₂/CO derived from all other states
351 that reported both species (a mean value). The spatial distribution of the nonroad FFCO₂ emissions followed two
352 approaches. Nonroad FFCO₂ emissions reported through the 2011 NEI point data source (5 locations, 12% of
353 nonroad FFCO₂ in the LA Megacity) are located in space according to the provided latitude and longitude.
354 Emissions reported through the county-scale nonroad data source utilize multiple spatial surrogates provided by the
355 EPA reflecting a series of spatial entities such as the mines, golf courses and agricultural lands. There were instances
356 in which nonroad FFCO₂ emissions could not be associated with a spatial entity due to missing data. These
357 emissions are spatialized by first aggregating all the offending sub-county emission elements within a county for a
358 given surrogate shape type (e.g., golf courses, mines) and then distributing these emissions evenly across the county.
359 To distribute the nonroad FFCO₂ emissions from the annual to hourly timescale, a series of surrogate time profiles
360 provided by the EPA are used. These temporal surrogates are comprised of three cyclic time profiles (diurnal,
361 weekly, monthly) specific to SCC that are combined to generate hourly SCC-specific time fractions for an entire
362 calendar year.

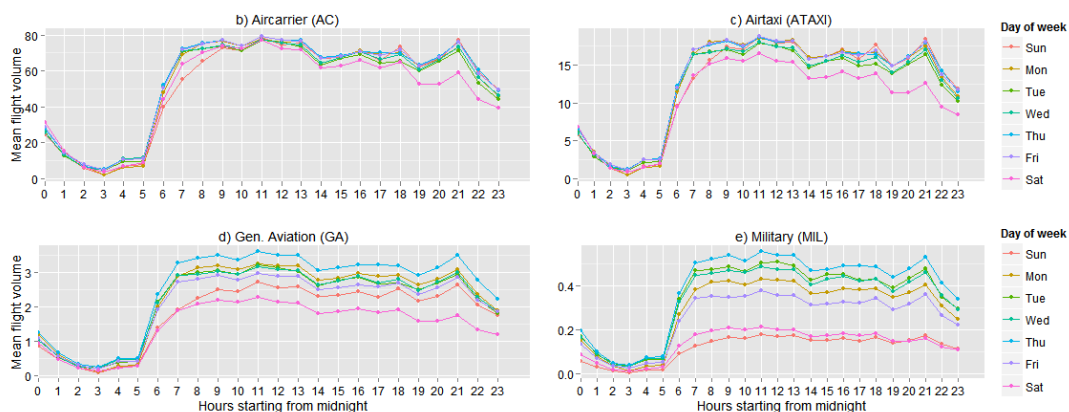
363 **2.3.6 Airport**

364 Emissions of FFCO₂ from airports retrieved from the Vulcan system for the Hestia-LA domain are specific to
365 geocoded airport locations. Hence, the Hestia-LA system performs the temporal distribution only. There are 374
366 commercial airports/helipads in the Hestia-LA domain totaling 0.77 MtC/year, dominated by Los Angeles County
367 (0.39 MtC/year), and LAX in particular.

368 The annual airport FFCO₂ emissions are distributed in time utilizing airport-specific flight volume data from four
369 datasets:

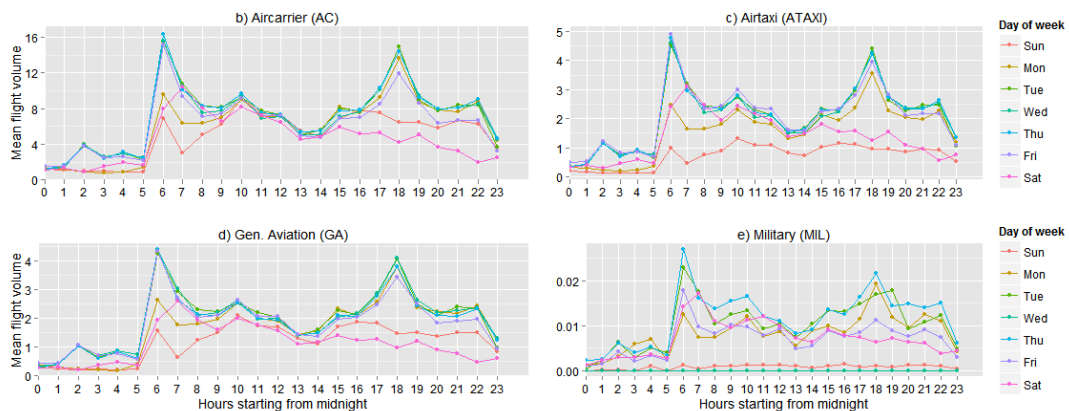
- 370 1) The Operations Network (OPSNET) data from the Federal Aviation Administration (FAA) which reports total
371 date-specific, daily flight volume (365 values) at specific airports for specific aircraft classes (FAA, 2018a);
- 372 2) "AIRNAV" data which reports average daily percentage flight volume for aircraft class at US airports and
373 facilities (Airnav.com, 2018);
- 374 3) The Enhanced Traffic Management System Counts (ETMSC) daily flight volume data from the FAA was for two
375 airports in the Hestia-LA domain (NTD and RIV) with mostly military operations (FAA, 2018b);
- 376 4) The Los Angeles World Airports (LAWA) data which reports hourly flight volume for Los Angeles International
377 airport (LAX), Ontario airport (ONT), and Van Nuys airport (VNY) (LAWA, 2014).

378 For three large airports (LAX, ONT, VNY), the daily aircraft class-specific flight volume (from OPSNET) and the
379 hourly data on flight volume (from LAWA) were combined to create hourly aircraft class-specific time profiles
380 (Figure 4-6). All of the flight volume data are specific to four aircraft classes: Military (MIL), Air Carrier (AC),
381 General Aviation (GA), and Air Taxi (AT).



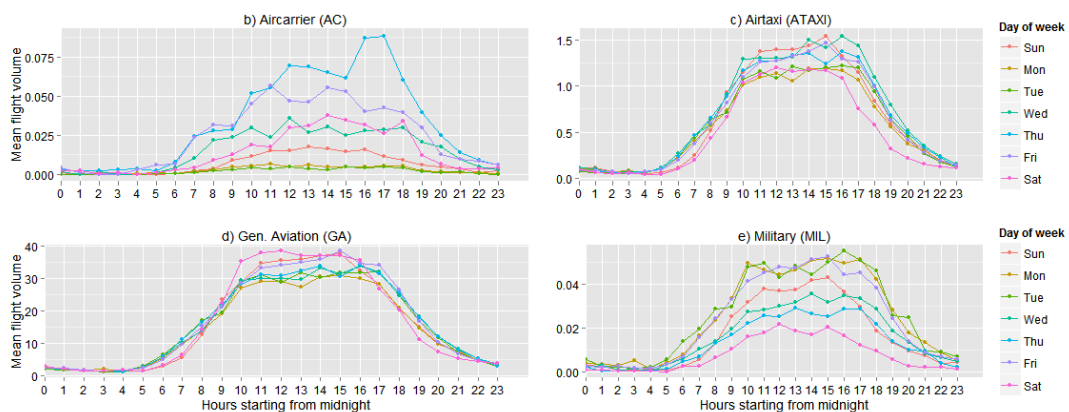
382
 383
 384
 385

Figure 4. Average hourly flight volume at LAX for a) total, b) AC, c) AT, d) GA, and e) MIL aircraft classes for each day of the week. The plots represent the mean diurnal cycle for all Mondays, Tuesday, Wednesdays, and so on, given a full year of data.



386
 387

Figure 5. Same as figure 4 but for the Ontario (ONT) airport.



388
 389

Figure 6. Same as figure 4 but for the Van Nuys (VNY) airport.



390 To generate hourly time profiles for all other airports in the Hestia-LA domain for which this type of detailed hourly
391 data was not available, airports first were categorized based on average daily flight volumes and average aircraft
392 class proportions from the OPSNET, AIRNAV and ETMSC data. Each airport was categorically matched to one of
393 the two non-international airports with hourly data (ONT, VNY) and the hourly time fractions adopted. LAX was
394 unique in terms of its volume and aircraft class proportions and hence was not used for any other airports. For
395 helipads and very small airports, a flat time structure was used.

396 2.3.7 Railroad

397 Railroad FFCO₂ emissions are similarly distributed in space within the Vulcan system and passed through to the
398 Hestia-LA landscape without alteration (see Gurney et al., 2018 for additional details). The Vulcan process treats
399 railroad point records somewhat differently from the railroad nonpoint records. The point source railroad emissions
400 are associated with rail yards and related geo-specific locales and are placed in space according to the provided
401 latitude and longitude. The railroad FFCO₂ emissions associated with the nonpoint 2011 NEI reporting contain an
402 ID variable that links to a spatial feature (rail line segment) in the EPA railroad GIS Shapefile. Nearly two-thirds of
403 the railroad emitting segments have no segment link. The sum of these “unlinked” railroad FFCO₂ emissions are
404 distributed to rail line within the given county according to freight statistics. The annual railroad FFCO₂ emissions
405 are distributed to the hourly timescale with no additional temporal structure (a “flat” time distribution).

406 2.3.8 Commercial marine vessels

407 The commercial marine vessel (CMV) FFCO₂ emissions retrieved from the Vulcan system are specific to county
408 and SCCs which are subsequently aggregated by the Hestia-LA system into emissions associated with two activity
409 categories: “port” emissions “underway”. For the port CMV emissions (Figure 7), a port Shapefile from the EPA
410 was used as a reference along with a visual inspection of the coastline (USEPA, 2015a).

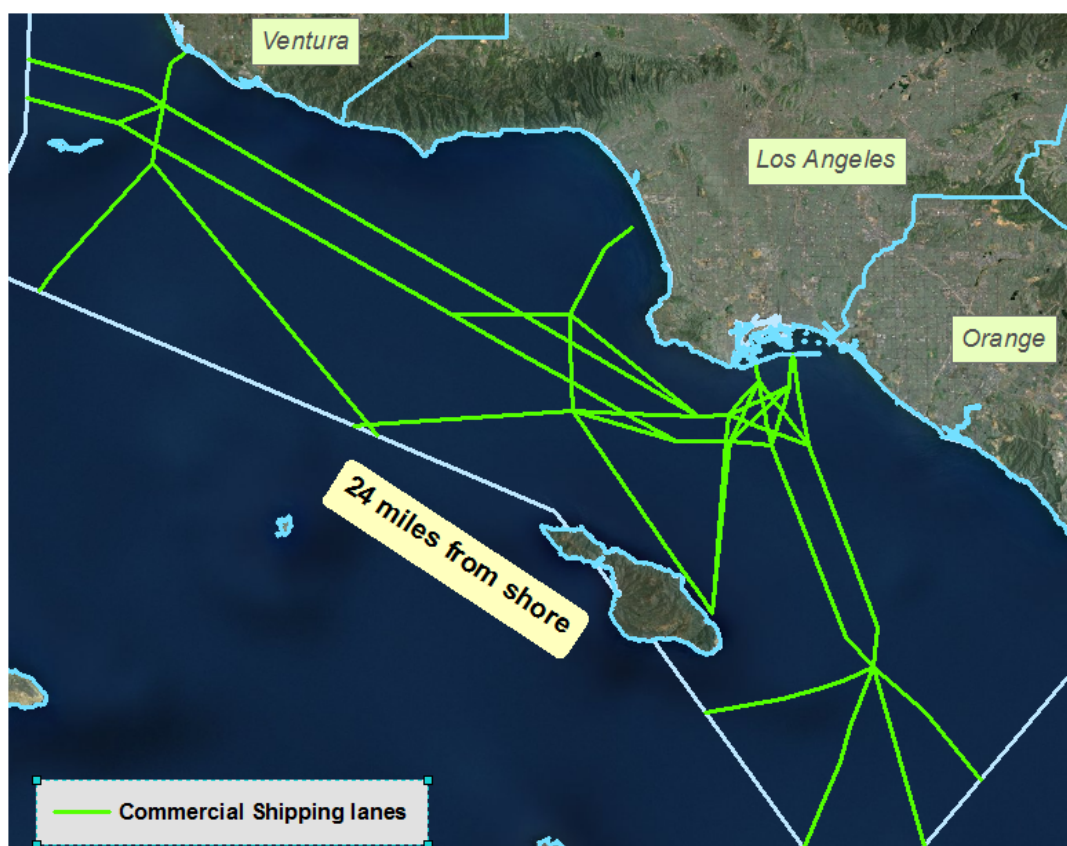


411

412 **Figure 7. The 6 ports in the Hestia-LA domain to which Vulcan FFCO₂ port emissions are allocated.**



413 Allocation of the FFCO₂ emissions designated as “underway” used a polyline Shapefile (Figure 8) of commercial
414 shipping lanes in California provided by CARB (Alexis, 2011). The shipping lanes for each county were bounded so
415 that only lanes between the exterior of ports and a distance of 24 miles from the port exterior, were included. County
416 total FFCO₂ emissions were then distributed evenly to these shipping lanes on a per unit length basis individually for
417 each of the three counties. Each shipping lane segment receives its length fraction of the annual total of underway
418 emissions.



419
420 **Figure 8. Commercial Marine Vessel (CMV) shipping lanes in the Hestia-LA to which Vulcan FFCO₂**
421 **underway emissions are allocated.**

422 The time profile was based on the Marine Emissions Model (MEM) developed by CARB. MEM had marine vessel
423 activity data which includes the arrival time of ocean-going vessels for all ports in California spanning the 2004 to
424 2006 time period (Alexis, 2011). This hourly dataset was analyzed using a Fourier time series which allowed for an
425 isolation of the dominant cycles of ship traffic in the data. Results from the Fourier fit were then used to fill in the
426 missing hours. Weekday hours were examined separately from weekend hours to isolate potential differences in
427 traffic volume. Three cycles resulted: a 24-hour diurnal cycle, a weekly cycle and a monthly cycle. These were
428 applied to all years of the annual FFCO₂ emissions to create an hourly distribution at each of the CMV ports within
429 the domain.



430 2.3.9 Cement

431 Emissions of FFCO₂ from cement production facilities retrieved from the Vulcan system for the Hestia-LA domain
432 are specific to geocoded facility locations. CO₂ is emitted from cement manufacturing as a result of fuel combustion
433 and as process-derived emissions [van Oss, 2005]. The emissions from fuel combustion are captured in the industrial
434 sector. The process-derived CO₂ emissions result from the chemical process that converts limestone to calcium
435 oxide and CO₂ during “clinker” production (clinker is the raw material for cement which is producing by grinding
436 the clinker material). These emissions are reported as cement sector emissions
437 These emissions are fully calculated, spatialized and temporalized in the Vulcan v3.0 system and passed directly to
438 the Hestia-LA landscape. The cement facilities are geocoded with some corrections to provide more accurate
439 placement of the emission stacks.

440 2.4 Gridding

441 The county-level FFCO₂ emissions inventory, which has been distributed into the point, line and polygon features
442 by sector, are rasterized into a sector-specific and time-resolved gridded form under a common grid reference. This
443 grid reference divides the entire Hestia-LA domain into 509-by-342 1 km x 1 km grid cells on the California State
444 Plane Coordinate System. The grid reference is made into “fishnet” in the Shapefile format with 509-by-342 square
445 geometries.

446 The first step of the gridding procedure is to perform a spatial intersection operation between the fishnet and each of
447 the sectoral emissions layers in ArcGIS. The output of an intersection operation is a new set of features common to
448 both input layers. The emissions value of each feature in the intersection output was scaled by the ratio of the spatial
449 footprint of the feature to that of the original feature in the sectoral emissions layer. For line-source and polygon-
450 source emissions layers, the spatial footprint represents the line length and polygon area respectively. For point-
451 source layers, the footprint is equal to 1.

452 2.5 Uncertainty

453 Uncertainty estimation for Hestia results are challenging owing to the fact that many of the datasets used to
454 construct the flux results are not accompanied by uncertainty or traceable to transparent sources or methods. The
455 approach taken for the Hestia-LA v2.5 results was to conservatively estimate the uncertainty based on available
456 comparisons to Hestia results and exploration of the dominant components of the Hestia output. The first of these is
457 a comparison of the Hestia-Indianapolis (Hestia-Indy) results to an inverse-estimation of fluxes in the INFLUX
458 project (Gurney et al., 2017). In that study, it was shown that the Hestia-Indy whole-city FFCO₂ emissions result
459 agreed with an inverse estimate (Lauvaux et al., 2016) within 3.3% (CI: -4.6% to +10.7%). This suggests both
460 potential bias (3.3%) and an estimation uncertainty (~7.5%). This comparison was accomplished by estimating
461 portions of the carbon budget, included in the inverse estimate, but not explicitly included in the Hestia-Indy result.
462 Most importantly, biosphere respiration estimated from chamber studies at commensurate urban latitudes combined
463 with a remote-sensing based approach to quantifying the available vegetated landscape. This comparison, it should
464 be noted, is for a single city (Indianapolis) for a single time period. We directly sum the random and systematic error
465 and use this in the current study to represent the Hestia-LA whole-city uncertainty (a 95% CI), rounded up to 11%.



466 The next element for consideration with a conservative uncertainty estimate is the work done to compare two
467 different electricity production FFCO₂ estimates in the US. This work (Gurney et al., 2016) found that one-fifth of
468 the facilities had monthly FFCO₂ emission differences exceeding -6.4%/+6.8% for the year 2009 (the closest
469 analyzed year to the 2011 analysis examined here). The distributions of emissions of the two datasets were not
470 normally distributed nor were the differences. Hence, a typical gaussian uncertainty estimate cannot be made –
471 rather, the difference distribution was represented by quintiles of percentage difference. Hence, these values cannot
472 be cast within the context of other normally-distributed errors. However, we conservatively consider the quintile
473 value (the positive and negative tails) as a one-sigma value and 13% as a two-sigma value. The contribution of
474 electricity production is important to urban FFCO₂ emissions uncertainty given how large power production can be
475 within the total urban FFCO₂ context. For example, in the Los Angeles Megacity electricity production accounts for
476 19% of the total FFCO₂ emissions. The percentage differences can act as a form of uncertainty at the pointwise or
477 (conservatively) the gridcell scale, though only representative of the type of uncertainties represented by electricity
478 production point sources.

479 Finally, an initial assessment of the range of two critical parameters in the Vulcan/Hestia estimation is included as
480 part of the conservative uncertainty estimation. The two critical parameters are the CO emissions factor and the CO₂
481 emissions factor. Primarily for the CO EF, there is a range of potential values for each application (combination of
482 fuel category and combustion technology) though that range is not represented by a well-populated distribution of
483 values, but rather a discrete set of values within the data sources described in Gurney et al. (2009). Furthermore, the
484 expectation is that the CO EFs would not be normally distributed even were there to be a well-populated distribution
485 of values (i.e. many literature estimates of the same fuel/combustion technology) owing to the nature of CO
486 emissions from fuel combustion. This is driven by both the variation in combustion conditions for a given
487 fuel/technology combination and the variation in CO EF values across combustion technology. The distribution
488 would likely be a positively skewed “heavy” or “long” tailed distribution. For the current study, a range of the CO
489 and CO₂ EF values culled from the literature are conservatively assigned a one-sigma uncertainty of 10% or a two-
490 sigma value of 20%. Like the electricity production analysis in the previous paragraph, the uncertainty associated
491 with the CO and CO₂ emission factors is a gridcell-scale uncertainty (as opposed to whole city where error
492 cancelation occurs) and is independent of the electricity production uncertainty estimate (the CO and CO₂ EF values
493 are not used in the electricity production sector but in the other point sources and nonpoint sources).

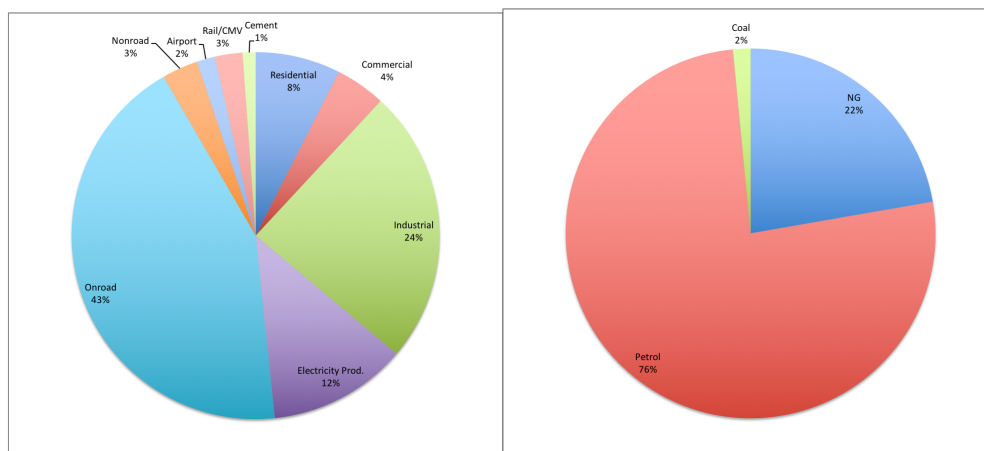
494 These latter two uncertainty are more representative of gridcell-scale uncertainties and sum them in quadrature to
495 arrive at a gridcell-scale uncertainty (95% CI) of 23.4% or conservatively rounded to 25%. Work is underway that
496 includes a complete input parameter range for the Hestia emissions data results to more formally assign uncertainty
497 at multiple scales.

498 **3 Results**

499 The total 2011 emissions for the Hestia-LA domain are 48.06 ± 5.3 MtC/yr (Figure 9, Table 5). Transportation
500 accounts for the largest share (24.27 ± 2.7 MtC/yr) of the total and within the transportation sector, onroad emissions
501 account for the largest portion (20.81 ± 2.3 MtC/yr). The next largest sectors are the industrial (11.65 MtC/yr ± 1.3)
502 and electricity production (5.88 ± 0.76 MtC/yr) sectors, respectively. Onroad, electricity production, residential and



503 industrial FFCO₂ emissions make up 86% of the total. Petroleum accounts for almost 75% of the total LA Megacity
 504 fuel consumption for direct FFCO₂ emissions consistent with the dominance of the transportation and industrial
 505 sectors which are mostly reliant on petroleum fuels. Los Angeles County dominates emissions in the five counties of
 506 the Hestia-LA domain accounting for 55% of the total FFCO₂ emissions. This is followed by San Bernardino,
 507 Orange, Riverside, and Ventura counties, respectively. Los Angeles and San Bernardino counties are dominated by
 508 onroad and industrial FFCO₂ emissions, while onroad emissions account for the largest share, by far, in the
 509 remaining three counties. Not surprisingly, Los Angeles county has the largest CMV FFCO₂ emissions among the
 510 five counties owing to the port of Los Angeles which hosts a large amount of international commercial shipping. At
 511 0.61 ± 0.067 MtC/yr, it rivals in emission magnitude the combination of residential and commercial building
 512 emissions in each of the other four counties.



513
 514 **Figure 9. Total FFCO₂ emissions proportions for the Hestia-LA domain. a) FFCO₂ emission proportions by**
 515 **sector; b) FFCO₂ emission proportions by fuel category.**

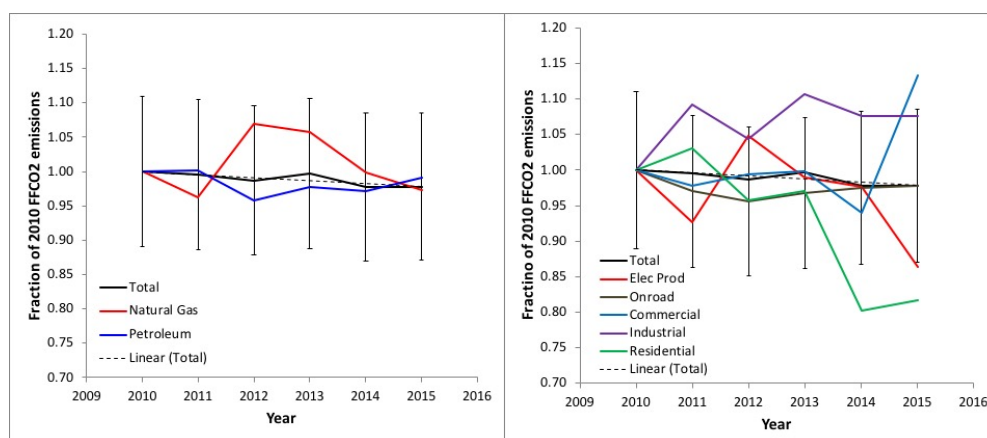
516 **Table 5. Sectoral FFCO₂ emissions in the five Hestia-LA domain counties for the year 2011. Units: MtC/yr.**

Sector	Los Angeles (MtC/yr)	Orange (MtC/yr)	San Bernardino (MtC/yr)	Riverside (MtC/yr)	Ventura (MtC/yr)	Total (MtC/yr)
Residential	2.00	0.64	0.40	0.36	0.20	3.59
Commercial	1.47	0.12	0.21	0.24	0.071	2.12
Industrial	7.27	0.94	2.99	0.25	0.20	11.65
Electricity production	2.73	0.69	1.54	0.71	0.21	5.88
Transportation	12.95	3.83	3.58	2.88	1.02	24.27
Onroad	11.03	3.46	2.98	2.51	0.82	20.81
Nonroad	0.79	0.27	0.19	0.19	0.087	1.52
Airport	0.39	0.06	0.14	0.11	0.070	0.77
Railroad	0.13	0.028	0.27	0.072	0.010	0.51
CMV	0.61	0.012	0	0	0.037	0.66
Cement	0	0	0.55	0.0077	0	0.55
Total	26.42	6.22	9.28	4.45	1.70	48.06

517 Total emissions in the LA Megacity show a small downward trend over the 2010-2015 time period of 0.44%/year
 518 which is a statistically significant trend (slope: -0.21 MtC/yr; CI: -0.397, -0.023). Individual sectors show greater
 519 variation there are compensating temporal changes among the individual sectors (Figure 10). The residential sector
 520 showed a relatively large decline in 2014, though due to its relatively small portion of total emissions, has limited



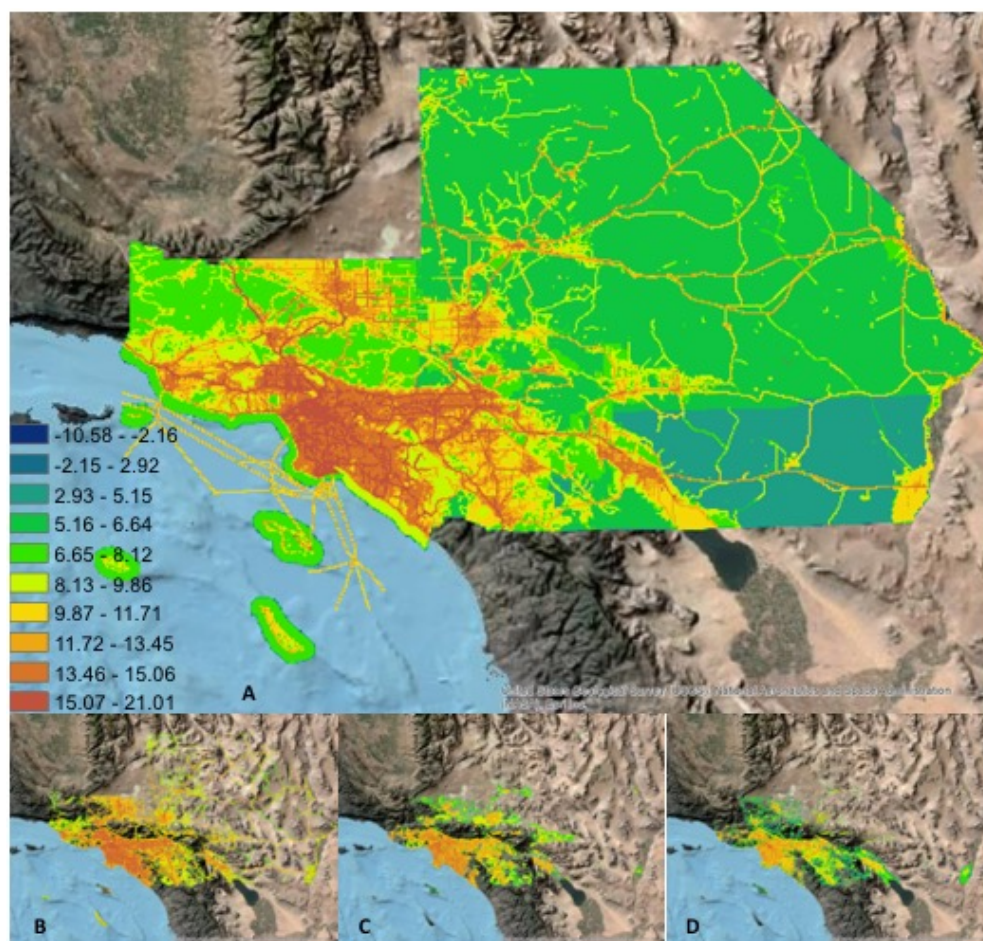
521 impact on the total temporal variation from 2010-2015. Similarly, 2015 showed a large increase in commercial
 522 sector emissions which also do not translate to large changes in the total FFCO₂ emissions time series. The relative
 523 temporal stability of the industrial and onroad FFCO₂ emissions sectors combined with their large share of the total
 524 FFCO₂ emissions are reflected in the total emissions trend. When categorized by fuel type, natural gas FFCO₂
 525 emissions exhibited the greatest variation with a maxima in 2012 and to a lesser extent 2013, driven primarily by
 526 consumption in the electricity production sector.



527
 528 **Figure 10. Fractional changes over the 2010 to 2015 timeframe in LA Basin FFCO₂ emissions. a) by fuel**
 529 **category; b) by sector. Whole-city error provided for the total FFCO₂ emissions only.**

530 Spatial distribution of the Hestia-LA FFCO₂ emissions demonstrate the importance of the populated areas and road-
 531 intensive portions of the domain in the overall emissions (Figure 11). The constant emissions that appear over large
 532 areas, particularly in San Bernardino and Riverside counties, are due to the nonroad FFCO₂ emissions which have
 533 relatively simple spatial distribution proxies with considerable areal extent.

534



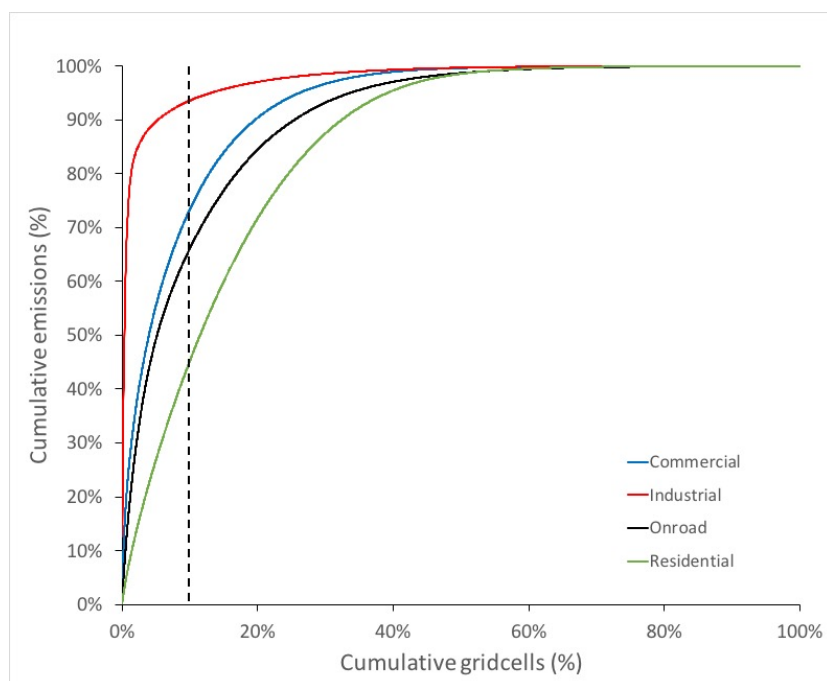
535

536 **Figure 11. Hestia-LA v2.5 FFCO₂ emissions for the year 2011 represented on a 1 km x 1 km grid. a) total**
537 **FFCO₂ emissions; b) onroad FFCO₂ emissions; c) residential FFCO₂ emissions; d) commercial FFCO₂**
538 **emissions. Units: natural logarithm KgC/gridcell/yr.**

539 Figure 12 shows the cumulative FFCO₂ emissions across four of the sectors for which the 1 km² gridcell
540 accumulation is most appropriate: the commercial, industrial, onroad, and residential sectors. The other FFCO₂
541 emission sectors (airport, electricity production, cement) are not included in Figure 12 because they are dominated
542 by a few points, have limited spatial distribution (railroad) or no spatial variance (nonroad). The accumulation of
543 FFCO₂ emissions at the threshold by which 10% of the gridcells are accumulated is noted on the figure. For the
544 industrial sector, 10% of the largest emitting gridcells account for 93.6% of the total industrial sector emissions. For
545 the commercial sector this occurs at 73.4% of the accumulated gridcells. For the onroad and residential sectors this
546 occurs at 66.2% and 45.3%, respectively. This demonstrates two important points about the FFCO₂ emissions in the
547 Los Angeles Megacity (and most cities). First, the emissions have very high spatial variance with few gridcells
548 accounting for a large portion of the total FFCO₂ emissions. Second, this is particularly true for the industrial sector,
549 driven by the fact that it is comprised of a large proportion of point emitters. This is somewhat true of the



550 commercial sector which does have some pointwise data within the original NEI reporting. Of the remaining two
551 sectors, which contain no pointwise spatial emitters, the majority (66.2%) of the onroad emissions are captured in
552 the largest 10% while the residential sector, being less concentrated, shows an accumulation just short of the 50%
553 threshold at a 10% gridcell accumulation threshold.

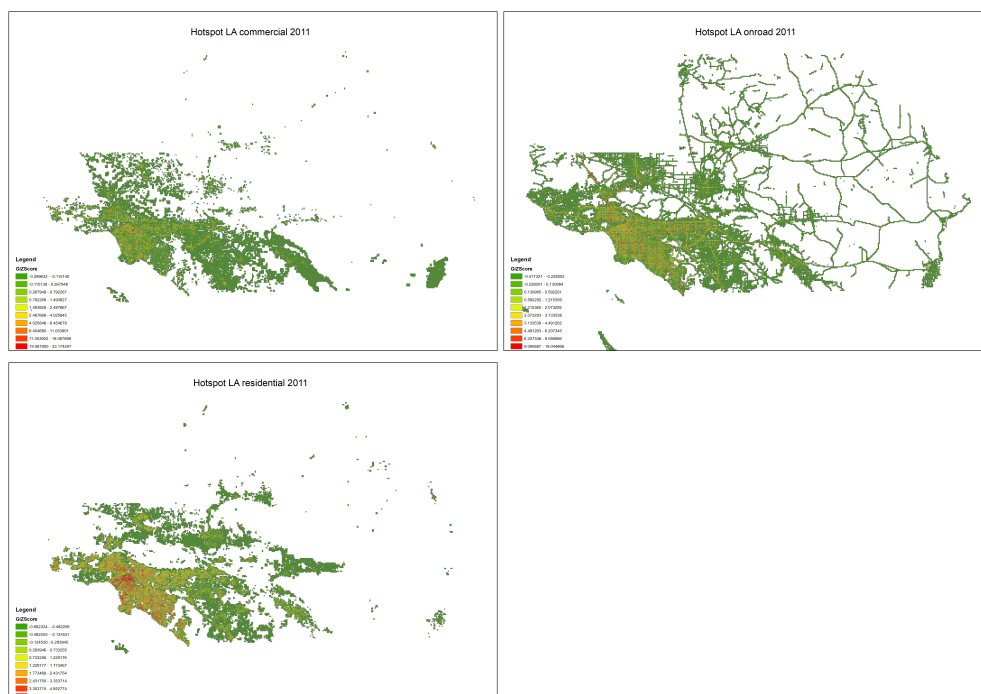


554
555 **Figure 12. Cumulative FFCO₂ emissions according to key sectors in the Hestia-LA FFCO₂ emissions data**
556 **product. The dashed line at 10% cumulative grid cells is given for reference. See text for details.**

557 An important attribute of estimating urban emissions at fine space and time scales is the resulting clustering in space
558 (and time) of the emissions and the varying patterns of the clustering across the emitting sectors. Figure 13 provides
559 an analysis of spatial clustering using the *Getis-Ord-Gi* statistic which provides a score that measures statistically
560 significant departures from random local clustering (*Getis and Ord, 1992*). The three sectors included in this
561 analysis are the residential, commercial and onroad sectors. The onroad sector shows a more widely dispersed
562 clustering pattern with local “hotspots” generated by high traffic flow points and traffic congestion, primarily on the
563 interstate network coincident with a greater density of commercial and residential activity. The residential sector
564 exhibits less extensivity compared to the onroad FFCO₂ emissions clustering but with larger individual hotspot
565 areas. Particularly large clustering occurs from the coast centered on Santa Monica and Marina del Rey and
566 extending East and North through West Hollywood on to Pasadena and Alhambra. Other hotspots occur in the
567 Manhattan Beach to Redondo Beach corridor, the Burbank and Glendale area and the coastal portion of Orange
568 county (e.g. Huntington Beach, Newport Beach). The commercial sector shows the a similar overall extensivity to
569 the residential sector but with less extensive individual hotspots associated with commercial building clusters.



570



571

572

573

Figure 13. The *Getis-Gi* z-score for Hestia-LA FFCO₂ emissions across three sectors; a) commercial; b) onroad; c) residential.

574

575

576

577

578

579

580

581

582

583

584

585

There are very few potential sources for comparison to the Hestia FFCO₂ emissions as few inventory efforts have been accomplished at the sub-state spatial scale in the United States. However, the Southern California Association of Governments (SCAG) have completed a regional greenhouse gas emissions inventory for a base year period of 1990-2009 with projections out to the year 2035 (SCAG, 2012). The SCAG inventory reflects two components that make comparison to the Hestia-LA FFCO₂ emissions data product imperfect. First, the domain considered in the SCAG inventory includes Imperial county, a county not included in the Hestia-LA domain. However, Imperial county is estimated to be less than a few percent of the SCAG domain total. For example, Imperial county onroad VMT is 1.9% of the SCAG domain total. The Imperial county retail sales of electricity is 1.1% of the SCAG domain total. The other distinction is that the SCAG inventory reports total GHGs, inclusive of both methane (CH₄) and nitrous oxide (N₂O). However, in the sectors and activities used in comparing the SCAG inventory to the Hestia-LA FFCO₂ emissions data product, both CH₄ and N₂O are negligibly small. Hence, small differences (<5%) could be due to these categorical discrepancies.

586

587

588

589

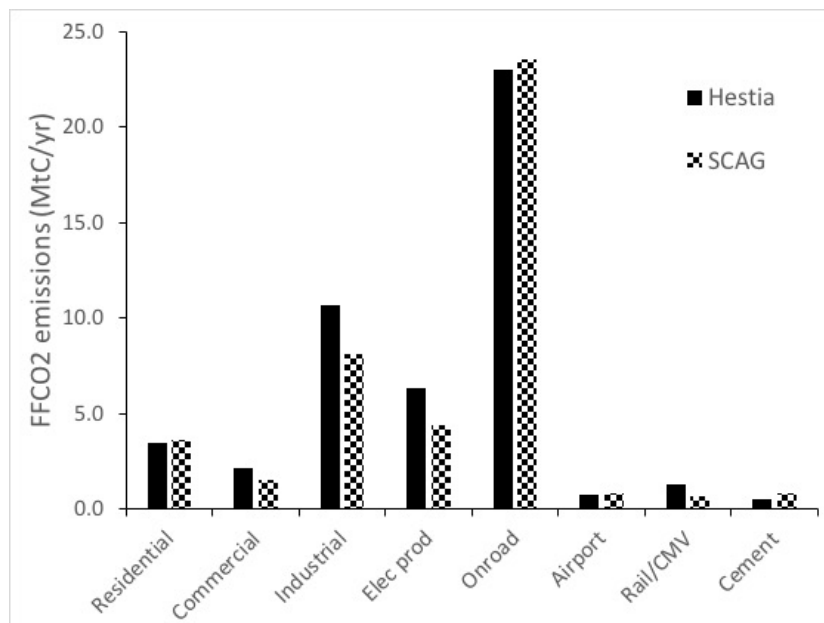
590

591

Figure 14 shows a 2010 comparison between the two estimates using the comparable sector divisions. The Hestia-LA FFCO₂ emissions estimate is 10.7% larger than the SCAG estimate, 95% of the difference (4.46 MtC/yr) owing to the larger industrial and electricity production FFCO₂ emissions in the Hestia estimate. We have included the nonroad sector in the onroad category as the SCAG inventory did not explicitly include a nonroad sector. SCAG documentation suggests that the nonroad sector is included in the forecasts for the residential, commercial and industrial sectors (SCAG, 2012, page C-10) but further details on the base year estimates could not be found and no



592 mention is made in the report where these sectors are described. If the Hestia nonroad estimate (1.56 MtC/yr) were
 593 not allocated to onroad but distributed to the residential, commercial and industrial sectors it would exacerbate the
 594 difference in the onroad, commercial and industrial sectors.



595
 596 **Figure 14. Comparison of sector-specific FFCO₂ emissions for the year 2010 between the Hestia-LA and**
 597 **SCAG estimates. Units: MtC/yr.**

598 The California Energy Commission archives energy consumption data for both natural gas and electricity
 599 (<http://ecdms.energy.ca.gov/>). The data is archived as specific to the residential sector and the non-residential sector.
 600 Because of ambiguities regarding the non-residential sector definition, we compare the reported values by county for
 601 the residential only (Table 6). Good agreement for natural gas FFCO₂ emissions is achieved for the Los Angeles
 602 Megacity as a whole (<1%) with some variation at the scale of the individual counties. Agreement with the CEC
 603 estimate is better than that found for the comparison with the SCAG inventory (Hestia being 3.1% lower than the
 604 SCAG residential NG FFCO₂ estimate).

605 **Table 6. Residential natural gas FFCO₂ emissions in the five Hestia-LA domain counties for the year 2011**
 606 **compared to estimates from the California Energy Commission (CEC). Units: MtC/yr.**

County	Hestia	CEC	diff (%)
Los Angeles	1.94	1.98	-2.0%
Orange	0.63	0.59	5.7%
San Bernardino	0.40	0.39	0.8%
Riverside	0.35	0.39	-11.1%
Ventura	0.19	0.18	6.5%
LA Megacity	3.51	3.54	-0.9%

607 Average hourly variations in FFCO₂ emissions are sensitive to both the sector and spatial location. Figure 15
 608 presents annual mean diurnal patterns specified by county and sector (the railroad or cement sectors were
 609 constructed with no diurnal cycle and hence is not shown). As noted previously, Los Angeles county shows the



610 greatest emissions overall, particularly for the commercial marine vessel sector where the port of Los Angeles
611 dominates. The commercial, residential, onroad and CMV sectors exhibit two maxima, one in the morning (~5-10
612 am, local time) and another in the afternoon/evening. In the commercial sector, this afternoon/evening maximum
613 occurs later in this time period centered on 9 pm local time, coinciding with retail closing schedules. The maximum
614 CMV emissions are shifted by roughly two hours earlier in the day for both the morning and afternoon/evening
615 peaks. The afternoon/evening maximum for the onroad sector shows an afternoon/evening maximum that is of
616 longer duration than that in the morning with emissions gradually rising after the midpoint of the day, local time. In
617 addition to large daily variations, the onroad sector contains a significant weekly temporal pattern with emissions
618 largest on Monday and smallest on Saturday (Figure 16).

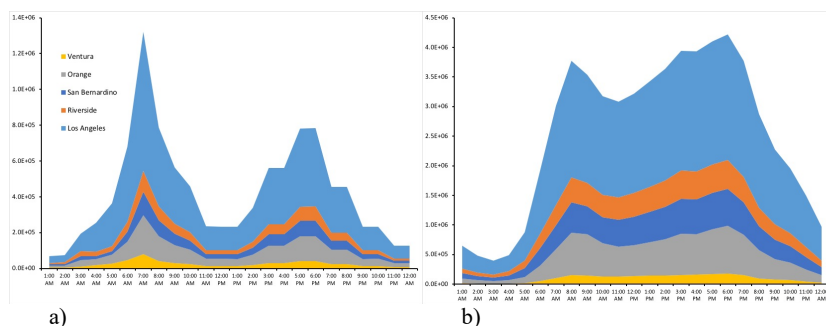
619 Diurnal patterns in onroad and airport FFCO₂ emissions have a single maximum at the middle of the day but broadly
620 extending across all daylight hours. In the case of the nonroad emissions, this is simply a reflection of the EPA
621 temporal surrogate applied. In the case of the airport FFCO₂ emissions, the time structure reflects the reported air
622 traffic volume at the major airports in the LA Megacity. Finally, the industrial and electricity production sectors
623 maintain relatively constant emissions across all 24 hours. In the case of the industrial sector, this reflects the
624 integration of industry-specific EPA temporal surrogates within a given county. For the electricity production sector,
625 the time structure is primarily driven by the stack-monitored emissions and shows a slightly greater emission in the
626 evening hours compared to all other hours.

627 The diurnal patterns are consistent across all five counties with the exception of the commercial sector where there
628 are small differences in the maximum point of the morning emissions in San Bernardino and Ventura counties
629 compared to the other LA Megacity counties.

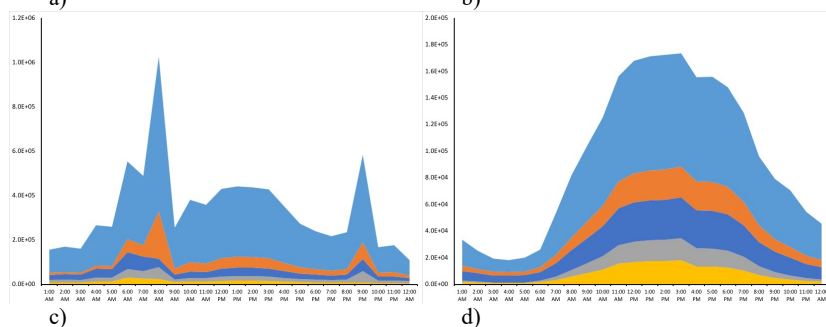
630



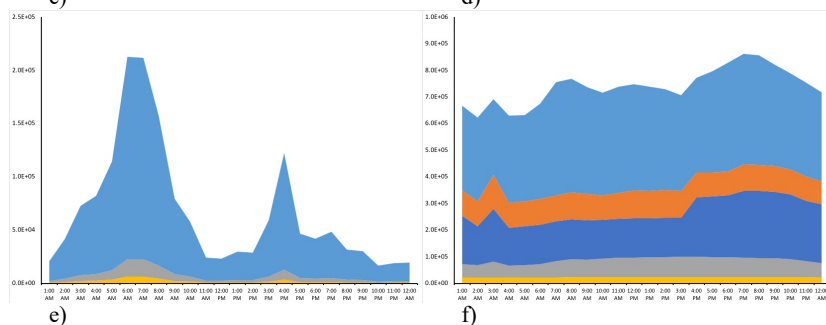
631
632



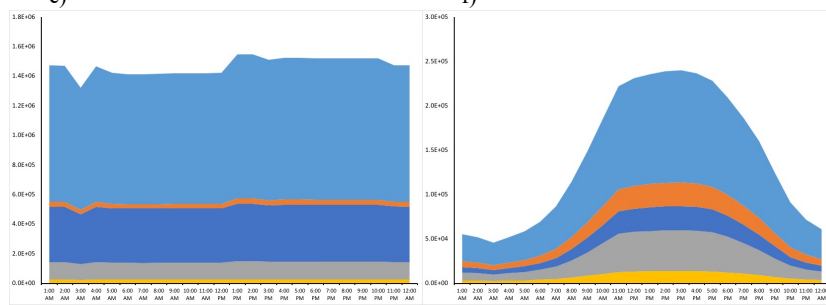
633
634



635
636



637



638

g)

h)

639

Figure 15. Average daily FFCO₂ emissions in the Hestia-LA v2.5 data product for five counties across eight

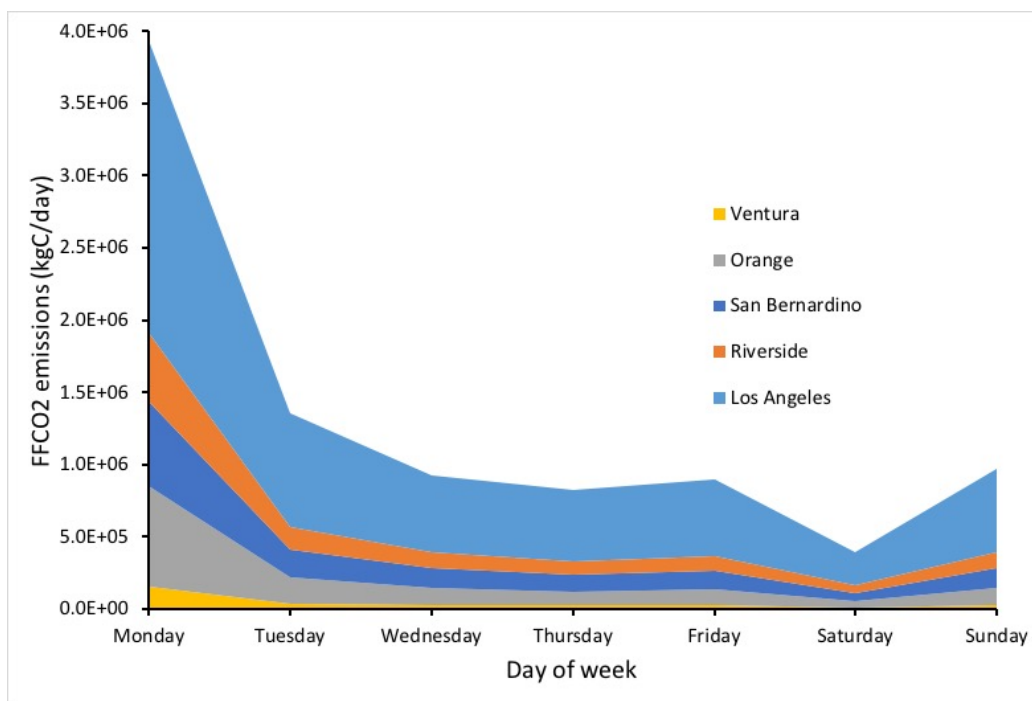
640

sectors. A) residential; b) onroad; c) commercial; d) airport; e) commercial marine vessel; f) electricity

641

production; g) industrial; h) nonroad. Note: different scale range on each plot. Units: kgC/hour.

642



643

644 **Figure 16. Average weekly onroad FFCO₂ emissions from the Hestia-LA v2.5 data product for five counties.**645 **Units: kgC/day**646 **4 Discussion**

647 The first Hestia urban FFCO₂ emissions data product was produced for the Indianapolis domain (Gurney et al.,
648 2012). As an outcome of the Hestia effort, a large multifaceted effort, the Indianapolis Flux Experiment (INFLUX),
649 emerged (Whetstone et al., 2017; Davis et al., 2017). INFLUX aims to advance quantification and associated
650 uncertainties of urban CO₂ and CH₄ emissions by integrating a high-resolution bottom-up emission data product,
651 such as Hestia, with atmospheric concentration measurements (Turnbull et al., 2015; Miles et al., 2017; Richardson
652 et al., 2017), flux measurements (Cambaliza et al., 2014; 2015; Heimberger et al., 2017), and atmospheric inverse
653 modeling. In addition to its use as a key constraint in the INFLUX atmospheric inverse estimation (Lauvaux et al.,
654 2016), Hestia has been informed by atmospheric observations making it useable as a standalone high-resolution flux
655 estimate offering a detailed space-time understanding of urban emissions. Begun in the late 2000s, INFLUX has
656 explored many aspects of the individual elements of a scientifically-driven urban flux assessment (e.g. Wu et al.,
657 2018) in addition to demonstrating potential reconciliation between Hestia and the atmospheric measurements
658 (Gurney et al., 2017; Turnbull et al., 2018). Similar efforts are ongoing in the Salt Lake City (Mitchell et al., 2016;
659 Lin et al., 2018) and Baltimore (Martin et al., 2018) domains with a different arrangement of atmospheric
660 monitoring and modeling. As with INFLUX, a Hestia FFCO₂ emissions data product was produced in each domain
661 (Patarasuk et al., 2016; Gurney et al., 2018).



662 The Hestia Los Angeles Megacity effort was developed under the Megacities Carbon Project framework
663 (<https://megacities.jpl.nasa.gov/portal/>). It was designed to serve the Megacities Carbon Project in a similar capacity
664 to its role in INFLUX. The Hestia-LA results are unique in that it is the first high-resolution spatiotemporally-
665 explicit inventory of FFCO₂ emissions centered over a megacity. Presented here at the 1 km² spatial and hourly
666 temporal resolution, the emissions can be represented at finer spatial scales down to the individual building, though
667 with higher uncertainty. While policy emphasis in California thus far has been focused on CH₄ emissions (Carranza
668 et al., 2017; Wong et al., 2016; Verhulst et al., 2017; Hopkins et al., 2016), work is ongoing to use the extensive
669 atmospheric CO₂ observing capacity in the Los Angeles domain (e.g. Newman et al., 2016; Wong et al., 2015;
670 Wunch et al., 2009) within an atmospheric CO₂ inversion. This will offer an important evaluation of the Hestia-LA
671 emissions for which limited independent evaluation is currently available.

672 The potential of the Hestia-LA FFCO₂ emissions to enable or assist with policymaking in the cities, counties or
673 metropolitan planning domain of the overall Southern California area is considerable. The traditional urban
674 inventory approach, such as accomplished by many cities as part of their climate action plans, are whole-city
675 accounts, often specific to sector, that follow one of a few inventory protocols. Given the challenges of data
676 acquisition and the idiosyncrasies of protocol choice and needs, the traditional urban inventories are difficult to
677 compare across cities and hence, aggregate reliably in a metropolitan domain such as the LA Megacity. Importantly,
678 without space and time explicit emissions information, they are difficult to calibrate with atmospheric measurements
679 and hence, evaluate against this important scientific constraint. The Hestia-LA FFCO₂ emissions approach attempts
680 to overcome these limitations to traditional inventory work. By quantifying emissions at the scale of individual
681 buildings and road segments, with process detail such as the sector, fuel, and combustion technology, Hestia results
682 can be organized according to most of the protocols in use by cities. This explicit space and time detail also allow
683 for calibration to atmospheric measurements, for which emission location and time structure is essential.

684 The state of California continues to lead the nation in climate policy with numerous legislative and executive orders
685 outlining both general reduction goals and specific policy instruments. The California Global Warming Solutions
686 Act (Assembly Bill 32) passed in 2006, specifies a statewide reduction in greenhouse gas emissions to 1990 levels
687 by the year 2020 (<https://www.arb.ca.gov/cc/ab32/ab32.htm>). Furthermore, the bill requires reporting and
688 verification of reductions in order to demonstrate compliance. Executive order B-30-15 and Senate Bill, SB 32 have
689 built on this with an aim to reduce emissions 40% below 1990 levels by 2030 and 80% below 1990 levels by 2050,
690 respectively (<https://www.gov.ca.gov/2015/04/29/news18938/>;
691 https://leginfo.ca.gov/faces/billTextClient.xhtml?bill_id=201520160SB32). Ultimately, much of the
692 specific action needed to meet these goals will rest upon local governments and authorities. Given that 87% of the
693 state population resides in urban areas and nearly half of state population resides in the Los Angeles Megacity, the
694 cities and counties that comprise the Los Angeles metropolitan area have a central role to play in achieving the
695 statewide climate change policy goals. The city of Los Angeles, the largest individual city in the metro region, has
696 specified goals consistent with the state commitments, expecting to reduce greenhouse gas emissions 35% below
697 1990 levels by the year 2030 (http://environmentla.org/pdf/GreenLA_CAP_2007.pdf). To meet these reduction
698 goals, policy actions will become increasingly difficult to achieve at no- or low-cost and economic efficiency will
699 become central to making policy choices.



700 The most important attribute of the Hestia-LA approach, therefore, is the potential it offers for targeting urban CO₂
701 reduction policy more efficiently. As shown in Figures 12 and 13, FFCO₂ emissions are highly variable in space and
702 typically cluster in concentrated areas. In choosing specific policy approaches and instruments, this offers Los
703 Angeles policymakers the ability to target specific neighborhoods, road segments, or commercial hubs, where
704 policies will achieve the greatest reduction for resources expended. This rests on the argument that specificity leads
705 to efficiency. As all cities, including those in the Los Angeles Megacity, move towards those aspects of carbon
706 emission reductions that are not part of the “low hanging fruit” policy instruments, competition for limited resources
707 and policy justification will increase. Having information that targets the most efficient and effective emission
708 reduction investments, established by independent rigorous scientific information, will be at a premium. For
709 example, if a small proportion of the commercial sector buildings in the LA Megacity account for a large proportion
710 of the FFCO₂ emissions, knowing the location of these buildings and targeting energy efficiency programs to those
711 buildings, may offer the most economically efficient route to emissions reductions in the commercial sector. A
712 similar argument can be made in the onroad sector due to the clustering of large onroad emitting gridcells and
713 specific road-class attributes (see Rao et al., 2017).

714 A number of caveats are worth mentioning in association with the Hestia-LA v2.5 FFCO₂ emissions results. With
715 Vulcan v3.0 as the starting point for the quantification in Hestia, errors in Vulcan will be passed to Hestia, with a
716 few exceptions. Of particular note are the industrial sector and more specifically, refining operations which have
717 limited emissions reporting. These remain difficult to quantify due to the range of CO emission factors representing
718 many of the combustion processes undertaken at these large and complex facilities. The uncertainty estimation
719 described remains limited and there are additional sources of uncertainty that must be quantified such as categorical
720 errors (e.g. mis-specification of fuel category or road class), errors in spatial accuracy and spatial error correlation.
721 Quantifying these contributions to the overall uncertainty presented here remain a task for future work.

722 **5 Data availability, policy and future updates**

723 The Hestia-LA v2.5 emissions data product can be downloaded from the data repository at the National Institute
724 of Standards and Technology (<https://doi.org/10.18434/T4/1502503>) and is distributed under Creative Commons
725 Attribution 4.0 International (CC-BY 4.0, <https://creativecommons.org/licenses/by/4.0/deed.en>). The Hestia-LA
726 v2.5 FFCO₂ emissions data product is provided as annual and hourly (local and UTC versions) 1 km x 1 km
727 NetCDF file formats, one file for each of the 6 years (2010-2015). The hourly files are approximately 2.9 GB each.
728 The annual files are 0.34 GB each.
729 Attempts will be made to update the Hestia-LA FFCO₂ emissions on a roughly bi-annual basis, depending upon
730 support, the availability of updates to the Vulcan FFCO₂ emissions data product, and updates to the additional data
731 sources described in this study.

732 **6 Conclusion**

733 The Hestia Project quantifies urban fossil fuel CO₂ emissions at high space- and time-resolution with application to
734 both scientific and policy arenas. We present here the Hestia-LA version 2.5 FFCO₂ emissions data product which



735 represents hourly, 1 km², sector-specific emissions for the five counties of the Los Angeles metropolitan area for the
736 2010 to 2015 time period. The methodology relies on the results of the Vulcan Project (version 3.0) further
737 enhancing and distributing emissions to the scale of individual buildings and road segments with local data sources
738 acquired from local government agencies. Each sector is quantified using data sources and spatial/temporal
739 distribution approaches distinct to the sector characteristics. The results offer a detailed view of FFCO₂ emissions
740 across the LA Megacity and point to the extreme spatial variance of emissions. For example, 10% of the 1 km²
741 emitting gridcells account for 93.6%, 73.4%, 66.2%, and 45.3% of the emissions in the industrial, onroad,
742 commercial, and residential sectors, respectively. We find that the LA Megacity emitted 48.06 ± 5.3 MtC/yr in the
743 year 2011, dominated by Los Angeles county (26.42 ± 2.9 MtC/yr) and from a sector-specific viewpoint, dominated
744 by the onroad sector (20.81 ± 2.3 MtC/yr). Hestia FFCO₂ emissions are 10.7% larger than the inventory estimate
745 generated by the local metropolitan planning agency, a difference that is driven by the industrial and electricity
746 production sectors. Good agreement is found (<1%) when comparing residential natural gas FFCO₂ emissions to
747 utility-based reporting at the county spatial scale. The largest temporal variations are found in the diurnal cycle with
748 the residential, commercial, onroad, and commercial marine vessel emissions showing to maxima, one in the
749 morning and a second in the afternoon/evening. Airport and nonroad emissions, by contrast show broad maxima
750 across the daylight hours. Finally, the industrial and electricity production sectors show little diurnal variation across
751 24 hours. The onroad sector also exhibits variation in the weekly distribution of emissions with maximum FFCO₂
752 emissions on Monday and minimum emissions on Saturday.

753 The Hestia-LA v2.5 FFCO₂ emissions data product offers the scientific and policymaking communities
754 unprecedented spatially and temporally-resolved information on FFCO₂ emission sources in the Los Angeles
755 Megacity. As part of the Megacities Carbon Project, future work includes incorporation into atmospheric CO₂
756 inversion research to further evaluate the Hestia-LA data product and improve estimation. Policymakers can use the
757 Hestia-LA results to better-understand FFCO₂ emissions at the human scale, offering the potential for improved
758 targeting of FFCO₂ reduction policy instruments. Finally, urban researchers can use Hestia-LA to explore a number
759 of important urban science questions such as how emissions intersect with other urban sociodemographic variables
760 such as income, education, housing size, or vehicle ownership.

761 The Hestia-LA data product is publicly available and will be updated with future years as data becomes available.

762 **Competing Interests.** The authors declare that they have no conflict of interest.

763 Acknowledgments. This research was made possible through support from the National Aeronautics and Space
764 Administration Carbon Monitoring System program, Understanding User Needs for Carbon Information project
765 (subcontract 1491755), the National Aeronautics and Space Administration grant NNX14AJ20G, the National
766 Institute of Standards and Technology grant 70NANB14H321 and 70NANB16H264, JPL's Strategic
767 University Research Partnership program, and the Trust for Public Land.

768 **References**

- 769 Ainsworth, M. (2014) Shapefile with AAWT data. Retrieved by personal communication from Mike Ainsworth
770 (AINSWORT@scag.ca.gov) and Cheryl Leising (leising@scag.ca.gov) at Transportation Planning Department,
771 SCAG Riverside Office.
- 772 AirNav.com. Data retrieved from: <http://www.airnav.com/airports/> (Aug 1, 2018).
- 773 Alexis, A. (2011), Marine Emissions Model, California Air Resources Board. personal communication with Andy
774 Alexis, July 6, 2011 (email: aalexis@arb.ca.gov). Retrieved from:
775 <https://www.arb.ca.gov/ports/marinevess/ogv/ogv1085.htm>
- 776 Bréon, FM, Broquet, G, Puygrenier, V, Chevallier, F, Xueref-Remy, I, et al. 2015 An attempt at estimat- ing Paris
777 area CO₂ emissions from atmospheric concentration measurements, *Atmos. Chem. Phys.*, **15**: 1707–1724.
778 <http://www.atmos-chem-phys.net/15/1707/2015/>, DOI: <https://doi.org/10.5194/acp-15-1707-2015>
- 779 Cambaliza, M. O. L., Shepson, P. B., Caulton, D. R., Stirm, B., Samarov, D., Gurney, K. R., Turnbull, J., Davis, K.
780 J., Possolo, A., Karion, A., Sweeney, C., Moser, B., Hendricks, A., Lauvaux, T., Mays, K., Whetstone, J.,
781 Huang, J., Razlivanov, I., Miles, N. L. and Richardson, S. J.: Assessment of uncertainties of an aircraft-based
782 mass balance approach for quantifying urban greenhouse gas emissions, *Atmos. Chem. Phys.*, **14**(17), 9029–
783 9050, doi:10.5194/acp-14-9029-2014, 2014.
- 784 Cambaliza, M. O. L., Shepson, P. B., Bogner, J., Caulton, D. R., Stirm, B., Sweeney, C., Montzka, S. a., Gurney, K.
785 R., Spokas, K., Salmon, O. E., Lavoie, T. N., Hendricks, A., Mays, K., Turnbull, J., Miller, B. R., Lauvaux, T.,
786 Davis, K., Karion, A., Moser, B., Miller, C., Obermeyer, C., Whetstone, J., Prasad, K., Miles, N. and
787 Richardson, S.: Quantification and source apportionment of the methane emission flux from the city of
788 Indianapolis, *Elem. Sci. Anthr.*, **3**, 37, doi:10.12952/journal.elementa.000037, 2015.
- 789 California Air Resources Board (2014) *EMFAC2014 Volume I – User’s Guide*, v1.0.7, April 30, 2014, California
790 Environmental Protection Agency Air Resources Board, Mobile Source Analysis Branch, Air Quality Planning
791 & Science Division. EMFAC data retrieved from: <https://www.arb.ca.gov/emfac/2014/>
- 792 California Energy Commission (2006) California Commercial End-Use Survey, CEC-400-2006-005. Retrieved
793 from: http://www.energy.ca.gov/ceus/2006_enduse.html (Aug 1, 2018).
- 794 Carranza, V., T. Rafiq, I. Frausto-Vicencio, F.M. Hopkins, K.R. Verhulst, P. Rao, R.M. Duren, C.E. Miller (2018)
795 Vista-LA: Mapping methane-emitting infrastructure in the Los Angeles megacity, *Earth Syst., Sci. Data*, **10**,
796 653-676, <https://doi.org/10.5194/essd-10-653-2018>.
- 797 Chavez, A., and A. Ramaswami, 2011: Progress toward low carbon cities: Approaches for transboundary GHG
798 emissions’ footprinting. *Carbon Management*, **2**(4), 471-482, doi: 10.4155/cmt.11.38.
- 799 Christen, A., 2014: Atmospheric measurement techniques to quantify greenhouse gas emissions from cities. *Urban*
800 *Climate*, **10**, 241-260, doi: 10.1016/j.uclim.2014.04.006.
- 801 Clark, S. S., and M. V. Chester, 2017: A hybrid approach for assessing the multi-scale impacts of urban resource
802 use: Transportation in Phoenix, Arizona. *Journal of Industrial Ecology*, **21**(1), 136-150, doi:
803 10.1111/jiec.12422.



- 804 Commercial Building Energy Consumption Survey (2016) 2012 CBECS microdata files and information, U.S.
805 Energy Information Administration. Data retrieved from:
806 <https://www.eia.gov/consumption/commercial/data/2012/index.php?view=microdata> (Aug 1, 2018).
- 807 Davis, K.J., A. Deng, T. Lauvaux, N.L. Miles, S.J. Richardson, D. Sarmiento, K.R. Gurney, R.M. Hardesty, A.
808 Brewer, P.B. Shepson, M.O. Cambaliza, C. Sweeney, J. Turnbull, J. Whetstone, A. Karion (2017) The
809 Indianapolis Flux Experiment (INFLUX): A test-bed for developing anthropogenic greenhouse gas
810 measurements, *Elem Sci Anth*, **5**(21), <https://www.elementascience.org/article/10.1525/elementa.188/>
- 811 Department of Energy/Energy Information Administration 2003 Electric Power Monthly March 2003 Energy
812 Information Administration, Office of Coal, Nuclear, and Alternate Fuels, US Department of Energy,
813 Washington D.C. 20585. DOE/EIA form 923 reporting data retrieved from:
814 <http://www.eia.gov/electricity/data/eia923> (July 27, 2018).
- 815 Department of Energy/Energy Information Administration (2018) State Energy Consumption Estimates 1960
816 through 2016, DOE/EIA-0214(2016), June 2018, Washington DC.
- 817 Djuricin, S., D. E. Pataki, and X. Xu, 2010: A comparison of tracer methods for quantifying CO₂ sources in an urban
818 region. *Journal of Geophysical Research*, **115**(D11), doi: 10.1029/2009jd012236.
- 819 Federal Aviation Administration (2018a), OPSNET Manual: http://aspmhelp.faa.gov/index.php/OPSNET_Manual
820 (Aug 1, 2018). Data retrieved from: <https://aspm.faa.gov/opsnet/sys/main.asp>.
- 821 Federal Aviation Administration (2018b), ETMSC Manual: http://aspmhelp.faa.gov/index.php/ETMSC_Manual
822 (Aug 1, 2018). Data retrieved from: <https://aspm.faa.gov/tfms/sys/main.asp> (Aug 1, 2018).
- 823 Federal Emergency Management Agency (2017) HAZUS database. Retrieved from:
824 <https://www.fema.gov/summary-databases-hazus-multi-hazard> (Aug 1, 2018).
- 825 Feng, S., Lauvaux, T., Newman, S., Rao, P., Ahmadov, R., Deng, A., Díaz-Isaac, L. I., Duren, R. M., Fischer, M. L.,
826 Gerbig, C., Gurney, K. R., Huang, J., Jeong, S., Li, Z., **Miller, C. E.**, O'Keefe, D., Patarasuk, R., Sander, S. P.,
827 Song, Y., Wong, K. W., and Yung, Y. L.: Los Angeles megacity: a high-resolution land-atmosphere modelling
828 system for urban CO₂ emissions, *Atmos. Chem. Phys.*, **16**, 9019-9045, [doi:10.5194/acp-16-9019-2016](https://doi.org/10.5194/acp-16-9019-2016), 2016.
- 829 Getis, A., & Ord, J. K. (1992). The analysis of spatial association by use of distance statistics. *Geographical*
830 *analysis*, **24**(3), 189-206.
- 831 Grimmond, C. S. B., T. S. King, F. D. Cropley, D. J. Nowak, and C. Souch, 2002: Local-scale fluxes of carbon
832 dioxide in urban environments: Methodological challenges and results from Chicago.
- 833 Gurney, K.R., D. Mendoza, Y. Zhou, M Fischer, S. de la Rue du Can, S. Geethakumar, C. Miller (2009) [The Vulcan](#)
834 [Project: High resolution fossil fuel combustion CO₂ emissions fluxes for the United States](#), *Environ. Sci.*
835 *Technol.*, **43**(14), 5535-5541, doi:10.1021/es900806c.
- 836 Gurney K R, Huang J and Coltin K 2014 Comment on quick, J C (2014) carbon dioxide emission tallies for 210 US
837 coal-fired power plants: a comparison of two accounting methods *J. Air Waste Manage. Assoc.* **64**: 73–79 *J. Air*
838 *Waste Manage. Assoc.* **64** 1215–7
- 839 Gurney, K.R., J. Huang and K. Coltin (2016) [Bias present in US federal agency power plant CO₂ emissions data and](#)
840 [implications for the US clean power plan](#), *Env. Res. Lett.*, **11**, 064005, doi: 10.1088/1748-9326/11/6/064005.



- 841 Gurney, K. R., J. Liang, R. Patarasuk, D. O’Keeffe, J. Huang, M. Hutchins, T. Lauvaux, J. C. Turnbull, and P. B.
842 Shepson, 2017: Reconciling the differences between a bottom-up and inverse-estimated FFCO₂ emissions
843 estimate in a large U.S. urban area. *Elementa: Science of the Anthropocene*, **5**, 44, doi: 10.1525/elementa.137.
844 Gurney, K.R., Liang, J, D.O. O’Keeffe, R. Patarasuk, M. Hutchins, J. Huang, P. Rao, and Y. Song (2018)
845 Comparison of Global Downscaled Versus Bottom-Up Fossil Fuel CO₂ Emissions at the Urban Scale in Four
846 US Urban Areas, *under review at J. Geophys. Res.-Atmos.*
- 847 Gurney K.R., J. Liang, D. O’Keeffe, J. Huang, Y. Song, P. Rao, T.M. Wong (2019), Hestia Fossil Fuel Carbon
848 Dioxide (FFCO₂) Data Product - Los Angeles Basin, Version 2.5, 1km grid,
849 <https://doi.org/10.18434/T4/1502503> (last accessed December 20, 2018).
- 850 Heimerlberger Heimburger, AMF, Shepson, PB, Stirn, BH, Susdorf, C, Turnbull, J, et al. 2017 Precision Assessment
851 for the Aircraft Mass Balance Method for Measurement of Urban Greenhouse Gas Emission Rates. *Elem Sci*
852 *Anth*: In press for the INFLUX Special Feature
- 853 Hirsch, J. & Associates (2004) *Energy Simulation Training for Design & Construction Professionals*. Retrieved
854 from: <http://doe2.com/download/equest/eQuestTrainingWorkbook.pdf> (Aug 1, 2018). eQuest model download
855 available from: <http://www.doe2.com/eQuest/> (Aug 1, 2018).
- 856 Homer, C.G., Dewitz, J.A., Yang, L., Jin, S., Danielson, P., Xian, G., Coulston, J., Herold, N.D., Wickham, J.D.,
857 and Megown, K., 2015, [Completion of the 2011 National Land Cover Database for the conterminous United](#)
858 [States-Representing a decade of land cover change information](#). *Photogrammetric Engineering and Remote*
859 *Sensing*, v. 81, no. 5, p. 345-354
- 860 Hopkins, F. M., Kort, E. A., Bush, S. E., Ehleringer, J., Lai, C., Blake, D., and Randerson, J. T.: Spatial pat-
861 terns and source attribution of urban methane in the Los Angeles Megacity, *J. Geophys. Res.-Atmos.*, 121, 2490–
862 2507, <https://doi.org/10.1002/2015JD024429>, 2016b
- 863 Hutyra, L. R., R. Duren, K. R. Gurney, N. Grimm, E. A. Kort, E. Larson, and G. Shrestha, 2014: Urbanization and
864 the carbon cycle: Current capabilities and research outlook from the natural sciences perspective. *Earth’s*
865 *Future*, **2**(10), 473-495, doi: 10.1002/2014ef000255.
- 866 Intergovernmental Panel on Climate Change “IPCC guidelines for national greenhouse gas inventories, Prepared by
867 the National Greenhouse Gas Inventories Programme” (IGES, Japan, 2006).
- 868 Jones, C., and D. M. Kammen, 2014: Spatial distribution of U.S. household carbon footprints reveals
869 suburbanization undermines greenhouse gas benefits of urban population density. *Environmental Science and*
870 *Technology*, **48**(2), 895-902, doi: 10.1021/es4034364.
- 871 Kort, E. A., C. Frankenberg, C. E. Miller, and T. Oda, 2012: Space-based observations of megacity carbon dioxide.
872 *Geophysical Research Letters*, **39**(17), doi: 10.1029/2012gl052738.
- 873 Lauvaux, T, Miles, NL, Richardson, SJ, Deng, A, Stauffer, D, et al. 2013 Urban emissions of CO₂ from Davos,
874 Switzerland: the first real-time moni- toring system using an atmospheric inversion tech-
875 *and Climatol.*, **52**: 2654–2668. DOI: <https://doi.org/10.1175/JAMC-D-13-038.1>
- 876 Lauvaux, T., Miles, N. L., Deng, A., Richardson, S. J., Cambaliza, M. O., Davis, K. J., Gaudet, B., Gurney, K. R.,
877 Huang, J., O’Keefe, D., Song, Y., Karion, A., Oda, T., Patarasuk, R., Razlivanov, I., Sarmiento, D., Shepson, P.,
878 Sweeney, C., Turnbull, J. and Wu, K.: High-resolution atmospheric inversion of urban CO₂ emissions during



- 879 the dormant season of the Indianapolis Flux Experiment (INFLUX), *J. Geophys. Res. Atmos.*, 121(10), 5213–
880 5236, doi:10.1002/2015JD024473, 2016.
- 881 Le Quéré, C., Andrew, R. M., Friedlingstein, P., Sitch, S., Pongratz, J., Manning, A. C., Korsbakken, J. I., Peters, G.
882 P., Canadell, J. G., Jackson, R. B., Boden, T. A., Tans, P. P., Andrews, O. D., Arora, V. K., Bakker, D. C. E.,
883 Barbero, L., Becker, M., Betts, R. A., Bopp, L., Chevallier, F., Chini, L. P., Ciais, P., Cosca, C. E., Cross, J.,
884 Currie, K., Gasser, T., Harris, I., Hauck, J., Haverd, V., Houghton, R. A., Hunt, C. W., Hurtt, G., Ilyina, T., Jain,
885 A. K., Kato, E., Kautz, M., Keeling, R. F., Klein Goldewijk, K., Körtzinger, A., Landschützer, P., Lefèvre, N.,
886 Lenton, A., Lienert, S., Lima, I., Lombardozi, D., Metzl, N., Millero, F., Monteiro, P. M. S., Munro, D. R.,
887 Nabel, J. E. M. S., Nakaoka, S.-I., Nojiri, Y., Padin, X. A., Peregón, A., Pfeil, B., Pierrot, D., Poulter, B.,
888 Rehder, G., Reimer, J., Rödenbeck, C., Schwinger, J., Séférian, R., Skjelvan, I., Stocker, B. D., Tian, H.,
889 Tilbrook, B., Tubiello, F. N., van der Laan-Luijkx, I. T., van der Werf, G. R., van Heuven, S., Viovy, N.,
890 Vuichard, N., Walker, A. P., Watson, A. J., Wiltshire, A. J., Zaehle, S., and Zhu, D.: Global Carbon Budget
891 2017, *Earth Syst. Sci. Data*, 10, 405–448, <https://doi.org/10.5194/essd-10-405-2018>, 2018.
- 892 Lin, J.C., Mitchell, M., Buchert, E., Crosman, E., Mendoza, D., Gurney, K., Patasuruk, R., Bowling, D., Pataki, D., Bares,
893 R., Fasoli, B., Catherine, D., Baasandorj, M., Jacques, A., Hoch, S., Horel, J., and Ehleringer, J 2018 CO₂ and
894 carbon emissions from cities: linkages to air quality, socioeconomic activity and stakeholders in the Salt Lake
895 City urban area, *Bull Am. Meteorological Soc.*, in review.
- 896 Los Angeles County (2016) Countywide Building Outlines – 2014 Update – Public Domain Release. Retrieved
897 from: [https://egis3.lacounty.gov/dataportal/2016/11/03/countywide-building-outlines-2014-update-public-](https://egis3.lacounty.gov/dataportal/2016/11/03/countywide-building-outlines-2014-update-public-domain-release/)
898 [domain-release/](https://egis3.lacounty.gov/dataportal/2016/11/03/countywide-building-outlines-2014-update-public-domain-release/) (Aug 1, 2018).
- 899 Los Angeles World Airports (2014), Personal communication: Norene Hastings, Environmental Supervisor, Los
900 Angeles World Airports, Environmental Services division, January 2014.
- 901 Manufacturing Energy Consumption Survey (2010) 2010 MECS Survey Data, U.S. Energy Information
902 Administration. Retrieved from: <https://www.eia.gov/consumption/manufacturing/data/2010/#r10> (Aug 1,
903 2018).
- 904 Martin, C.R., N Zeng, A. Karion, K. Mueller, S. Ghosh, I. Lopez-Coto, K.R. Gurney, T. Oda, K. Prasad, Y. Liu,
905 R.R. Dickerson, J. Whetstone (2018), Investigating Sources of Variability and Error in Simulations of Carbon
906 Dioxide in an Urban Region, *submitted to Atmospheric Environment*.
- 907 Mays, K.L., Shepson, P.B., Stirn, B.H., Karion, A., Sweeney, C., et al. 2009 Aircraft-Based Measure-
908 ments of the Carbon Footprint of Indianapolis. *Environmental Science & Technology*, 43(20): 7816–7823. DOI:
909 <https://doi.org/10.1021/es901326b>
- 910 McKain, K., A. Down, S. M. Raciti, J. Budney, L. R. Hutyra, C. Floerchinger, S. C. Herndon, T. Nehrkorn, M. S.
911 Zahniser, R. B. Jackson, N. Phillips, and S. C. Wofsy, 2015: Methane emissions from natural gas infrastructure
912 and use in the urban region of Boston, Massachusetts. *Proceedings of the National Academy of Sciences USA*,
913 112(7), 1941–1946, doi: 10.1073/pnas.1416261112.
- 914 Menzer, O., W. Meiring, P. C. Kyriakidis, and J. P. McFadden, 2015: Annual sums of carbon dioxide exchange over
915 a heterogeneous urban landscape through machine learning based gap-filling. *Atmospheric Environment*, 101,
916 312–327, doi: 10.1016/j.atmosenv.2014.11.006.



- 917 Miles, N.L., Richardson, S.J., Lauvaux, T., Davis, K.J., Deng, A., et al. 2017a Quantification of urban atmospheric
918 boundary layer greenhouse gas dry mole fraction enhancements: Results from the Indianapolis Flux Experiment
919 (INFLUX), *Elem Sci Anth*: In press for the INFLUX Special Feature.
- 920 Mitchell, L., J.C. Lin, D.R. Bowling, D.E. Pataki, C. Strong, A.J. Schauer, R. Bares, S.E. Bush, B.B. Stephens, D.
921 Mendoza, D. Mallia, L. Holland, K.R. Gurney, J.R. Ehleringer (2018) Long-term urban carbon dioxide
922 observations reveal spatial and temporal dynamics related to urban characteristics and growth, *Proceedings of*
923 *the National Academy of Sciences*. March 5, 2018, <https://doi.org/10.1073/pnas.1702393115>
- 924 Mount, D.M. and S. Arya (2010) ANN: A Library for Approximate Nearest Neighbor Searching, Version 1.1.2,
925 Release Date: Jan 27, 2010. Retrieved from: <https://www.cs.umd.edu/~mount/ANN/> (Aug 1, 2018).
- 926 Newman, S., Xu, X., Gurney, K. R., Hsu, Y. K., Li, K. F., Jiang, X., Keeling, R., Feng, S., O’Keefe, D., Patarasuk,
927 R., Wong, K. W., Rao, P., Fischer, M. L., and Yung, Y. L.: Toward consistency between trends in bottom-up
928 CO₂ emissions and top-down atmospheric measurements in the Los Angeles megacity, *Atmos. Chem. Phys.*,
929 16, 3843–3863, <https://doi.org/10.5194/acp-16-3843-2016>, 2016.
- 930 Patarasuk, R., Gurney, K. R., O’Keefe, D., Song, Y., Huang, J., Rao, P., Buchert, M., Lin, J. C., Mendoza, D., and
931 Ehleringer, J. R.: Urban high-resolution fossil fuel CO₂ emissions quantification and exploration of emission
932 drivers for potential policy applications, *Urban Ecosyst.*, 19, 1013–1039, [https://doi.org/10.1007/s11252-016-](https://doi.org/10.1007/s11252-016-0553-1)
933 [0553-1](https://doi.org/10.1007/s11252-016-0553-1), 2016.
- 934 Porse, E., J. Derenski, H. Gustafson, Z. Elizabeth, and S. Pincetl, 2016: Structural, geographic, and social factors in
935 urban building energy use: Analysis of aggregated account-level consumption data in a megacity. *Energy*
936 *Policy*, **96**, 179–192, doi: 10.1016/j.enpol.2016.06.002.
- 937 Portland Cement Company, Economic Research Department (2006) *U.S. and Canadian Portland Cement Industry*
938 *Plant Information Summary*, Portland Cement Association, Skokie, IL.
- 939 Quick J 2014 Carbon dioxide emission tallies for 210 US coal-fired power plants: a comparison of two accounting
940 methods *J. Air Waste Manage. Assoc.* 64 73–9
- 941 Performance Measurement System (PeMS) Data Source: <http://www.dot.ca.gov/trafficops/mpr/source.html> (Aug 1,
942 2018).
- 943 Ramaswami, A., T. Hillman, B. Janson, M. Reiner, and G. Thomas, 2008: A demand-centered, hybrid life-cycle
944 methodology for city-scale greenhouse gas inventories. *Environmental Science and Technology*, **42**(17), 6455–
945 6461, doi: 10.1021/es702992q.
- 946 Rao, P., Gurney, K. R., Patarasuk, R., Yang, S., Miller, C. E., Duren, R. M., and Eldering, A.: Spatio-temporal
947 variations in on-road CO₂ emissions in the Los Angeles Megacity, *AIMS Geosci.*, 3, 239–267,
948 <https://doi.org/10.3934/geosci.2017.2.239>, 2017.
- 949 Residential Energy Consumption Survey (2013) 2009 RECS Survey Data, U.S. Energy Information Administration.
950 Retrieved from: <https://www.eia.gov/consumption/residential/data/2009/index.php?view=microdata> (Aug 1,
951 2018).
- 952 Richardson Richardson, S.J., Miles, N.L., Davis, K.J., Lauvaux, T., Martins, D., et al. 2017 CO₂, CO, and CH₄ surface in
953 situ measurement network in support of the Indianapolis FLUX (INFLUX) Experiment. *Elem Sci Anth*: Under
954 review for the INFLUX Special Feature.



- 955 Schwandner et al.
- 956 Seto, KC, Dhakal, S, Bigio, A, Blanco, H, Delgado, GC, et al. 2014 Human Settlements, Infrastructure and Spatial
957 Planning. In: *Climate Change 2014: Mitigation of Climate Change*. Contribution of Working Group III to the
958 Fifth Assessment Report of the Intergovernmental Panel on Climate Change [Edenhofer, O, Pichs-Madruga, R,
959 Sokona, Y, Farahani, E, Kadner, S, Seyboth, K, Adler, A, Baum, I, Brunner, S, Eickemeier, P, Kriemann, B,
960 Savolainen, J, Schlömer, S, von Stechow, C, Zwickel, T and Minx, JC (eds.)]. Cambridge University Press,
961 Cambridge, United Kingdom and New York, NY, US.
- 962 Shu, Y., and N. S. N. Lam, 2011: Spatial disaggregation of carbon dioxide emissions from road traffic based on
963 multiple linear regression model. *Atmospheric Environment*, **45**(3), 634-640, doi:
964 10.1016/j.atmosenv.2010.10.037.
- 965 Southern California Association of Governments (2012) Parcel Data GIS Shapefiles. Retrieved by personal
966 communication from Kimberly S. Clark (Clark@scag.ca.gov) and Christine Fernandez
967 (fernandez@scag.ca.gov).
- 968 Southern California Association of Governments (2014) SCAG AWDT data, personal communication, Mike
969 Ainsworth (AINSWORT@scag.ca.gov), Transportation Modeling, Air Quality & Conformity, October, 2014.
- 970 Turnbull, J. C., Sweeney, C., Karion, A., Newberger, T., Lehman, S. J., Tans, P. P., Davis, K. J., Lauvaux, T., Miles,
971 N. L., Richardson, S. J., Cambaliza, M. O., Shepson, P. B., Gurney, K., Patarasuk, R. and Razlivanov, I.:
972 Toward quantification and source sector identification of fossil fuel CO₂ emissions from an urban area: Results
973 from the INFLUX experiment, *J. Geophys. Res. Atmos.*, 120(1), 292–312, doi:10.1002/2014JD022555, 2015.
- 974 United States Environmental Protection Agency (1995) FIRE Version 5.0 Source Classification Codes and Emission
975 Factor Listing for Criteria Air Pollutants, EPA-454/R-95-012. Retrieved from
976 <https://www3.epa.gov/ttn/chief/old/efdocs/454r95012.pdf> (July 27, 2018).
- 977 United States Environmental Protection Agency (2013) Facility Registry Service (FRS). Setting Up A Data Flow
978 with FRS: FRS Information Needs. Retrieved from [https://www.epa.gov/frs/setting-data-flow-frs-](https://www.epa.gov/frs/setting-data-flow-frs-information-needs)
979 [information-needs](https://www.epa.gov/frs/setting-data-flow-frs-information-needs) (Aug 1, 2018).
- 980 United States Environmental Protection Agency (2014a), Motor Vehicle Emission Simulator (MOVES) User Guide
981 for MOVES2014, EPA-420-B-14-055. Retrieved from [https://www.epa.gov/moves/moves2014a-latest-version-](https://www.epa.gov/moves/moves2014a-latest-version-motor-vehicle-emission-simulator-moves)
982 [motor-vehicle-emission-simulator-moves](https://www.epa.gov/moves/moves2014a-latest-version-motor-vehicle-emission-simulator-moves) (July 27, 2018).
- 983 United States Environmental Protection Agency (2015a) Technical Support Document (TSD) Preparation of
984 Emissions Inventories for the Version 6.2, 2011 Emissions Modeling Platform. Retrieved from
985 <https://www.epa.gov/air-emissions-modeling/2011-version-62-technical-support-document> (July 27, 2018).
- 986 United States Environmental Protection Agency (2015b) 2011 National Emissions Inventory, version 2 Technical
987 Support Document. Document retrieved from [https://www.epa.gov/air-emissions-inventories/2011-national-](https://www.epa.gov/air-emissions-inventories/2011-national-emissions-inventory-nei-technical-support-document)
988 [emissions-inventory-nei-technical-support-document](https://www.epa.gov/air-emissions-inventories/2011-national-emissions-inventory-nei-technical-support-document) (July 27, 2018). NEI version 2.0 data retrieved from:
989 <https://www.epa.gov/air-emissions-inventories/2011-national-emissions-inventory-nei-data> (July 27, 2018).
- 990 United States Environmental Protection Agency (2015c), 40 DFR Part 60, EPA-HQ-OAR-2013-0602; FRL-XXXX-
991 XX-OAR, RIN 2060-AR33, Carbon Pollution Emission Guidelines for Existing Stationary Sources: Electric
992 Utility Generating Units, August 3, 2015. Air Markets Program Data 2012 Pre-packaged data retrieved from:
993 <ftp://ftp.epa.gov/dmdnload/emissions/hourly/monthly/> (May 28, 2012).



- 994 USGS (2003) *Minerals Yearbook, Vol. 1, Metals and Minerals, 2002*. U.S. Geological Survey. U.S. Department of
995 the Interior. July 2003
- 996 VandeWeghe, J. R., and C. Kennedy, 2007: A spatial analysis of residential greenhouse gas emissions in the
997 Toronto census metropolitan area. *Journal of Industrial Ecology*, **11**(2), 133-144, doi: 10.1162/jie.2007.1220.
- 998 Velasco, E., and M. Roth, 2010: Cities as net sources of CO₂: Review of atmospheric CO₂ exchange in urban
999 environments measured by eddy covariance technique. *Geography Compass*, **4**(9), 1238-1259, doi:
1000 10.1111/j.1749-8198.2010.00384.x.
- 1001 Velasco, E., S. Pressley, E. Allwine, H. Westberg, and B. Lamb, 2005: Measurements of CO₂ fluxes from the
1002 Mexico City urban landscape. *Atmospheric Environment*, **39**(38), 7433-7446, doi:
1003 10.1016/j.atmosenv.2005.08.038.
- 1004 Verhulst, K. R., Karion, A., Kim, J., Salameh, P. K., Keeling, R. F., Newman, S., Miller, J., Sloop, C., Pongetti, T.,
1005 Rao, P., Wong, C., Hopkins, F. M., Yadav, V., Weiss, R. F., Duren, R. M., and Miller, C. E.: Carbon dioxide
1006 and methane measurements from the Los Angeles Megacity Carbon Project – Part 1: calibration, urban en-
1007 hancements, and uncertainty estimates, *Atmos. Chem. Phys.*, **17**, 8313–8341, [https://doi.org/10.5194/acp-17-](https://doi.org/10.5194/acp-17-8313-2017)
1008 [8313-2017](https://doi.org/10.5194/acp-17-8313-2017), 2017
- 1009 Whetstone, J.R. (2018) Advances in urban greenhouse gas flux quantification: The Indianapolis Flux Experiment
1010 (INFLUX). *Elem Sci Anth*, **6**: 24. DOI: <https://doi.org/10.1525/elementa.282>
- 1011 Wong, C. K., Pongetti, T. J., Oda, T., Rao, P., Gurney, K. R., Newman, S., Duren, R. M., Miller, C. E., Yung, Y.
1012 L., and Sander, S. P.: Monthly trends of methane emissions in Los Angeles from 2011 to 2015 inferred by
1013 CLARS-FTS observations, *Atmos. Chem. Phys.*, **16**, 13121–13130, [https://doi.org/10.5194/acp-16-](https://doi.org/10.5194/acp-16-13121-2016)
1014 [13121-](https://doi.org/10.5194/acp-16-13121-2016)
2016, 2016.
- 1015 Wong, K. W., Fu, D., Pongetti, T. J., Newman, S., Kort, E. A., Duren, R., Hsu, Y.-K., Miller, C. E., Yung, Y. L.,
1016 and Sander, S. P.: Mapping CH₄ : CO₂ ratios in Los Angeles with CLARS- FTS from Mount Wilson,
1017 California, *Atmos. Chem. Phys.*, **15**, 241–252, <https://doi.org/10.5194/acp-15-241-2015>, 2015
- 1018 Wu, K, Lauvaux, T, Davis, KJ, Deng, A, Lopez Coto, I, Gurney, KR and Patarasuk, R 2018 Joint inverse estimation
1019 of fossil fuel and biogenic CO₂ fluxes in an urban environment: An observing system simulation experiment to
1020 assess the impact of multiple uncertainties. *Elem Sci Anth*. DOI: <http://doi.org/10.1525/elementa.138>
- 1021 Wunch, D., Wennberg, P. O., Toon, G. C., Keppel-Aleks, G., and Yavin, Y. G.: Emissions of greenhouse gases from
1022 a North American megacity, *Geophys. Res. Lett.*, **36**, 1–5, <https://doi.org/10.1029/2009GL039825>, 2009.
- 1023 Zhou, Y. Y., and K. R. Gurney, 2011: Spatial relationships of sector-specific fossil fuel CO₂ emissions in the United
1024 States. *Global Biogeochemical Cycles*, **25**, GB3002, doi: 10.1029/2010gb003822.